Canadian Mineralogist
Vol. 26, pp. 567-587 (1988)

MINERALOGY, COMPOSITION, AND FLUID-INCLUSION MICROTHERMOMETRY OF SEAFLOOR HYDROTHERMAL DEPOSITS IN THE SOUTHERN TROUGH OF GUAYMAS BASIN, GULF OF CALIFORNIA

JAN M. PETER AND STEVEN D. SCOTT
Marine Geology Research Group, Department of Geology, University of Toronto, Toronto, Ontario M5S 1A1

ABSTRACT

Numerous hydrothermal spires and mounds composed of carbonates, sulfates, silicates, metal (Fe, Zn, Cu, Fe, Pb) sulfides and iron oxides occur at 2000 m water depth in the sediment-filled Southern Trough of Guaymas Basin, Gulf of California. Predominant minerals include calcite, barite, amorphous silica, stevensite, pyrrhotite and marcasite. Major components (>1%) from bulk chemical analyses are Fe, Si, Ca, Ba, CO_2, S and SO_3 (and, for some samples, Pb, Zn, Al, Na and Mg). The Guaymas hydrothermal deposits therefore are fundamentally different from sulfide-rich deposits at sediment-free spreading axes. Microthermometric measurements of aqueous, two-phase inclusions in calcite from chimneys indicate trapping temperatures from about 150 to 315°C, and salinities of 3.7 to 8.1 (mean 5.4) equiv. wt.% NaCl. Trapping temperatures are in good agreement with temperatures of venting fluids measured *in situ* by thermocouple probe. Fluid-inclusion salinities cannot be reconciled with salinities measured from presently venting hydrothermal fluid and suggest that there are temporal variations in the chemistry of the vent fluid. Differences in salinity and homogenization temperatures for primary and secondary inclusions of individual chimneys require that there has been mixing of hot hydrothermal fluid and cold ambient seawater within chimneys and spires. Mineral assemblages and compositions of individual minerals can best be explained by mixing of end-member hydrothermal fluid with seawater. Most minerals are precipitated at the vent site largely in response to decreasing temperature induced by mixing with seawater.

Keywords: Guaymas Basin, hydrothermal precipitates, mineralogy, geochemistry, fluid inclusions, Gulf of California.

SOMMAIRE

De nombreuses cheminées hydrothermales et des amoncèlements de carbonates, sulfates, silicates, sulfures (de Fe, Zn, Cu, Fe et Pb) et oxydes de fer se trouvent à une profondeur d'eau de 2000 m dans la dépression du Sud, située dans le bassin de Guaymas (golfe de la Californie). Les espèces minérales les plus importantes sont calcite, barytine, silice amorphe, stevensite, pyrrhotite et marcasite. Les composants principaux (>1%), d'après les résultats d'analyses chimiques globales, sont Fe, Si, Ca, Ba, CO_2, S et SO_3 (et, dans certains cas, Pb, Zn, Al, Na et Mg). Sont aussi présents, en concentrations moins importantes (<1%): Zn, Pb, Na, Cu, Ag, As, Cd, Mn, Sb, Se et Sr. Des mesures microthermométriques d'inclusions aqueuses à deux phases dans la calcite des cheminées révèlent des températures de piégeage entre environ 150 et 315°C, et des salinités entre 3.7 et 8.1% (en poids; 5.4%, en moyenne) en équivalents de NaCl. Les températures de piégeage sont en bon accord avec les températures des émissions de fluides des évents, mesurées *in situ* par thermocouple. Toutefois, les salinités des inclusions fluides diffèrent sensiblement des valeurs typiques des fluides émis des évents actuels, et indiquent donc des variations séculaires dans la composition du fluide hydrothermal. En conclusion, les différences en salinité et en températures d'homogénéisation des inclusions fluides primaires et secondaires dans une seule cheminée indiquent la présence d'un mélange de fluide hydrothermal avec l'eau de mer ambiante et plus froide, à l'intérieur des cheminées. La meilleure explication des assemblages minéralogiques et de la composition des espèces minérales implique un mélange d'un fluide hydrothermal non-dilué avec l'eau de mer. La plupart des minéraux ont été précipités à l'orifice, surtout à cause d'un refroidissement de la solution dû au mélange.

(Traduit par la Rédaction)

Mots-clés: précipités hydrothermaux, minéralogie, géochimie, inclusions fluides, bassin de Guaymas, golfe de la Californie.

INTRODUCTION

Guaymas Basin is a hydrothermally active seafloor-spreading segment (Lonsdale *et al.* 1980) in the central Gulf of California (Fig. 1). The basin consists of two northeast-trending grabens termed the Northern and Southern Troughs, each about 40 and 20 km long, respectively, and 3 to 4 km wide. These were identified by Lonsdale & Becker (1985) to be a pair of en echelon, axial rift valleys that overlap at a non-transform offset (Lonsdale 1985). The basin floor is covered with biogenic and terrigenous sediments (Calvert 1966) at least 500 m thick (Lonsdale & Lawver 1980). Sedimentation rates of 1–2 m/1000 yrs (Calvert 1966) are unusually high. The terrigenous component is derived predominantly from Tertiary volcanics of the Mexican mainland. The abundant diatom remains in the central Gulf are a product of the area's prolific plankton blooms (Calvert 1966) which, together with the low oxygen concentration in the bottom water and reducing conditions in the sediment, are responsible for the 3–4% total organic carbon content of the sediments (Goldhaber 1974). Ocean-plate accretion occurs through dyke and sill intrusions into the unconsolidated muds (Einsele *et al.* 1980, Einsele 1982, 1985, 1986).

The first evidence for hydrothermal activity within Guaymas Basin was from heat-flow measurements

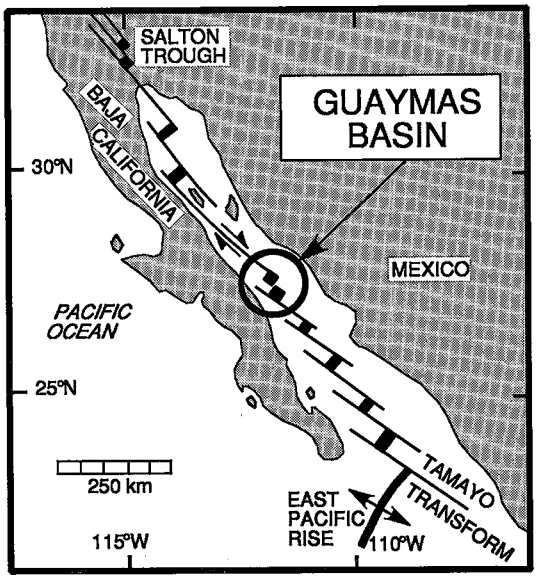

FIG. 1. Map of Gulf of California showing location of Guaymas Basin.

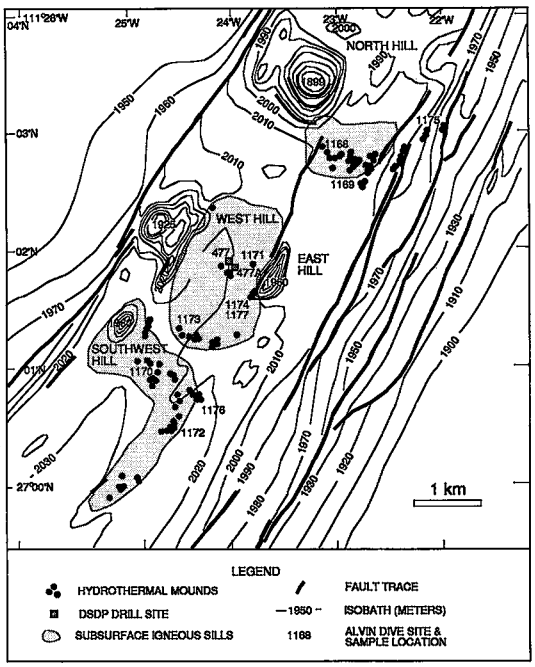

FIG. 2. Map of part of Southern Trough of Guaymas Basin showing location of hydrothermal deposits mapped by deep-tow side-scan sonar, and dive sites from 1982 ALVIN expedition (modified from Scott 1985).

which locally exceeded 1.2 Wm^{-2} in the sediments (Lawver *et al.* 1975, Lawver & Williams 1979, Williams *et al.* 1979). In 1977, ferromanganese-encrusted sulfide and talc deposits were discovered during submersible dives in the Northern Trough (Lonsdale 1978, Lonsdale *et al.* 1980). In addition, ^3He values in the Guaymas Basin were found to be 65–70% higher than atmospheric levels, indicating input from mantle sources (Lupton 1979). During Leg 64 of the Deep Sea Drilling Project (DSDP), three sites were drilled in the Guaymas Basin (sites 477/477A and site 481 in the Southern and Northern Troughs, respectively), and one (site 478) in the basin between the troughs (Fig. 2). Cores recovered hemipelagic sediments which were hydrothermally altered and intruded by basalt and dolerite sills of apparently very limited lateral extent (Einsele *et al.* 1980, Einsele 1985). Subsequently, in August 1980, extensive hydrothermal deposits were mapped by deep-tow side-scan sonar and photography (Lonsdale 1980). Samples of these hydrothermal precipitates were collected by dredge in 1980, and their mineralogy was described by Koski *et al.* (1985).

In January 1982, a series of nine dives by the submersible ALVIN in which Scott participated was conducted in the Southern Trough within the area of very high heat flow (Lonsdale & Becker 1985). Numerous hydrothermal mounds, chimneys, and spires, some actively venting hydrothermal fluids, were mapped, and samples of hydrothermal fluids and chimney and mound material were collected. In August 1985, the site was revisited by ALVIN with Peter participating. This paper describes the mineralogy, bulk composition, and fluid inclusions of samples recovered during the 1982 submersible dives. A subsequent paper (Peter, Shanks & Scott, in prep.) deals with the stable isotope geochemistry of these samples.

DESCRIPTION OF THE DEPOSITS

Beneath the floor of the Southern Trough are zones of anomalously shallow acoustic penetration where intrusive heating has induced unusually shallow lithification with abrupt boundaries that are assumed to delineate the limits of the sills. It is only over these areas of high conductive heat flow that hydrothermal deposits and plumes have been located within a 2 × 6 km area centered on 27°03′N, 111°23′W (Lonsdale & Becker 1985). Figure 2 shows the dive sites and the locations of most of the more than 130 hydrothermal deposits which Lonsdale & Becker (1985) noted in five main fields. Individual deposits are generally elongate northeast–southwest and cluster in lines parallel to faults (Fig. 2) thought to provide the main plumbing system that supplies the hydrothermal fluids to the sediments (Lonsdale & Becker 1985). The deposits have two end-member morphologies: mounds, and chimneys or spires. Gra-

dations between these were observed. The exposed portions of the mounds are conservatively estimated to constitute some 500,000 tonnes of mineral precipitates (Peter 1986).

Hydrothermal mounds are generally 5–25 m high and 10–50 m across, are steep-sided, and locally are covered by a dense mat of tubeworms. The whitish color of these mounds contrasts with the browns and reds of sulfide-rich mounds typically found on sediment-starved ridge crests. Figure 3a shows the top of a typical mound photographed from ALVIN. The limited illumination prevented acquisition of good panoramic photographs of an entire mound.

Large angular blocks of talus are scattered about the base of many mounds, and construction of mounds from talus may be an important process. Many mounds also have one or several horizontal "eaves" (*e.g.*, Fig. 3c) which protrude like skirts around their edges. Eaves are about 10 cm thick, 0.5 to 2 m wide, have a flat upper surface, and generally protrude laterally or curve slightly downward. Such eaves have also been described by Lonsdale & Becker (1985) who noted that these, as well as smaller eaves on chimneys or spires, are hollow and contain hot overpressured water which vents from a highly porous undersurface (Fig. 3b,c). Figure 4c shows the subhorizontal internal layering within one of these eaves.

Hydrothermal fluid from mounds escapes via chimney structures and through small fractures. In many instances, excavation of a mound with ALVIN's manipulator arm initiated venting, indicating that hot water is circulating inside. Close to mounds, the normal brownish hemipelagic and terrigenous sediment is overlain by distinctly reddish brown ochrous sediment up to about 1 cm thick. This flocculant is presumably the oxidized hydrothermal fallout from vent fluids escaping into seawater.

Chimneys and spires are columnar structures (Fig. 3a,b) that vary greatly in height from a few cm to >30 m. They are either directly on hydrothermal mounds, on lithified sediment close to hydrothermal mounds, or in isolated clusters far from any mounds. Chimneys have a central orifice up to several cm in diameter (Fig. 4a,b); in contrast, spires lack a central orifice but contain numerous holes or interconnecting pores (< 1 mm to 1 cm in diameter) through which hydrothermal fluid escapes. Unless otherwise indicated, the general term spire is used to refer both to chimneys and spires. Active and inactive spires can be further subdivided into two groups: carbonate + sulfate-rich, and sulfide-rich. Most spires encountered on submersible dives were inactive. Of those that were active, only a few were venting sulfide-particle-laden fluid of the kind typified by the "black smokers" at 21°N East Pacific Rise (EPR), and most were venting cloudy, greyish fluid. The highest exit temperature measured for vent fluids

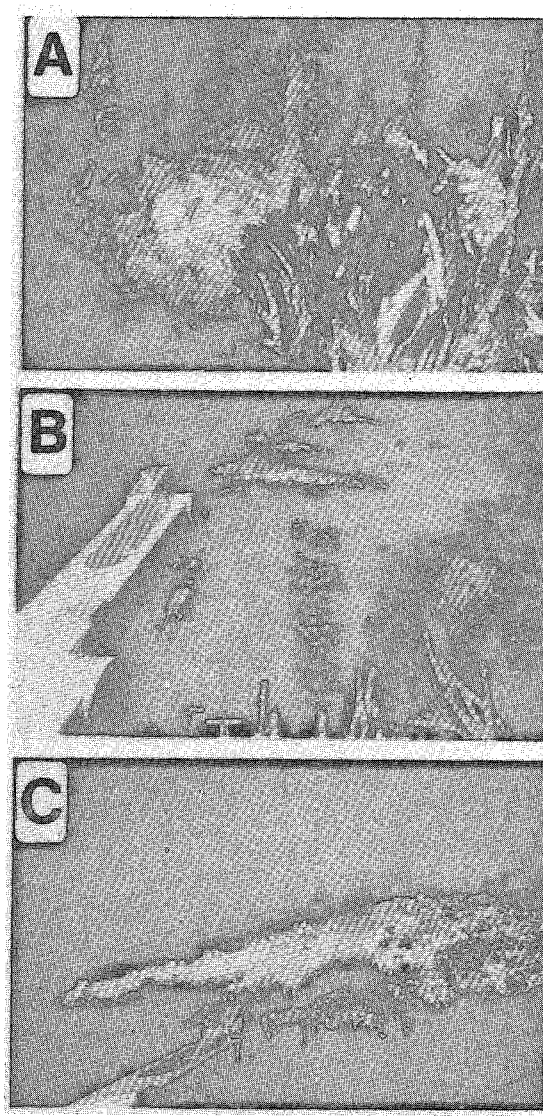

FIG. 3. ALVIN bow photographs of chimneys, spires, and mounds: A) spires on a mound; B) pagoda-like chimney. ALVIN's manipulator arm has broken off a piece of the eave and allowed hydrothermal fluid to effuse. C) Close-up of hydrothermal fluid escaping from the underside of a chimney eave. Manipulator arm is in foreground.

in Guaymas Basin on either of the expeditions was 359°C at a seafloor pressure of 200 bars (H. Jannasch, pers. comm.). Many spires are of the variety typified in photographs and illustrations of the 21°N EPR site (slender, tapering, with a central orifice), whereas others are delicate and castellate (Fig. 3b). Some spires display prominent eaves which project up to several tens of cm from the wall. The close

stacking of several eaves forms elaborate pagoda-like structures (Fig. 3b).

Many of the spires, and some mounds, are saturated with petroleum derived from thermal alteration of sedimentary organic material (Simoneit & Lonsdale 1982). Preliminary assessment does not reveal any relationship among sample type, temperature of venting fluid, and degree of oil saturation. In rare instances, venting hydrothermal fluids were seen to carry droplets of oil from the vent orifice. Oil stains impart a dark brown color to the normal mottled grey-white exterior of spires. Oxidation further imparts an orange-brown color that is more pronounced on inactive spires than active ones.

Analytical Methods

Spires were toppled and collected with ALVIN's manipulator arm, whereas mound samples were excavated with the manipulator. Such sampling procedures are acceptable for spires, but mound samples are not representative of the mound interior. About 100 kg of hydrothermal mineral precipitates were collected, with the largest piece weighing about 20 kg. The carcinogenic petroleum, as well as any seawater remaining in the sample, were removed by placing the samples in methanol to remove water, and then in methylene chloride to extract the petroleum. The petroleum acted as a binder in many samples and, when this was removed, some samples fell apart.

The mineralogy of the samples was determined by X-ray diffractometry (XRD), reflected and transmitted light microscopy, and scanning electron microscopy. In all, 41 polished thin sections, 17 polished specimens, and 32 fluid-inclusion sections were examined. Mineral separates for XRD were obtained either by hand-picking or by separation in

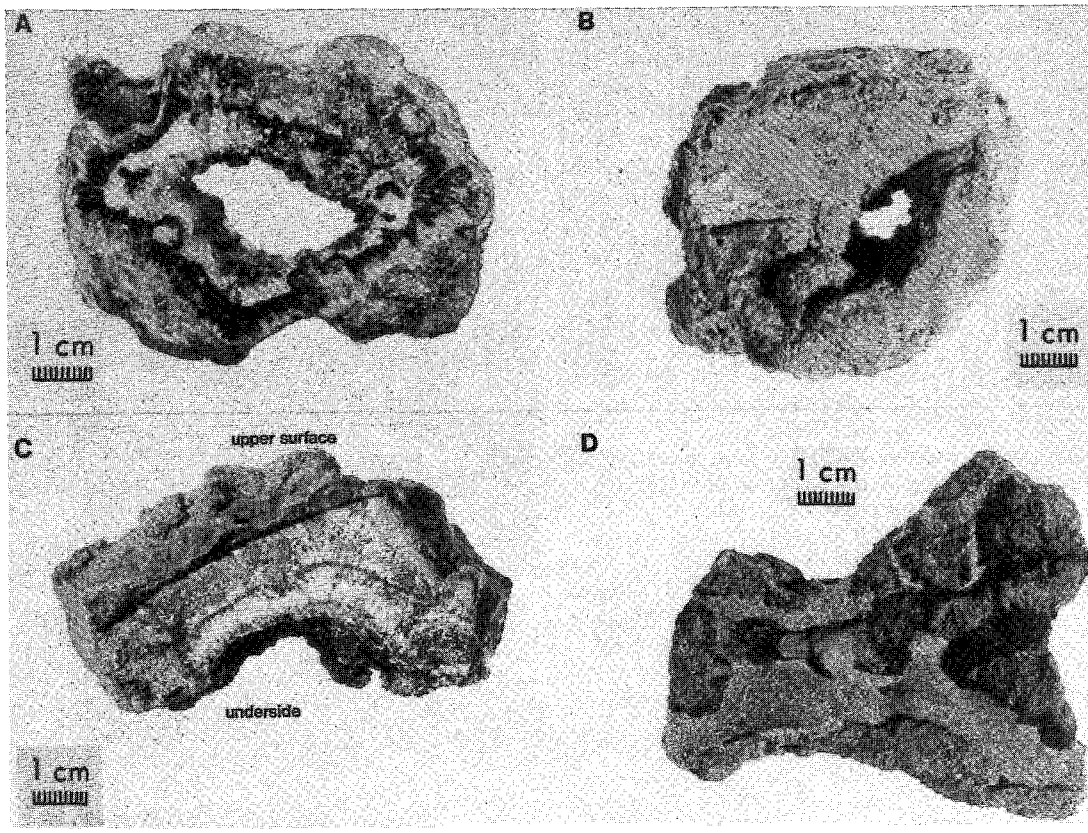

FIG. 4. A) Cross-sectional slab of chimney 1173-6. Narrow concentric zones of metal sulfides (dark grey) occur in the middle of the wall. Calcite (white) lines the orifice. B) Cross-sectional slab of chimney 1169-1B. Chimney is composed predominantly of calcite with minor sulfides. C) Cross-sectional slab of chimney eave 1174-5C. Underside is lined with pyrrhotite plates. Another such zone of pyrrhotite is located about 0.75 cm from the underside. White is predominantly calcite, and medium-grey upper surface is a coating of iron oxide. D) Undersurface of chimney eave 1173-10 showing delicate pyrrhotite plates (dark) oriented perpendicular to the eave and calcite (white) growth surface.

a heavy liquid. Several samples were thermally treated and glycolated to check for the presence of smectite. Minerals were analyzed using an ETEC automated microprobe equipped with an energy-dispersion analyzer. Operating conditions and standards are given in Peter (1986).

Fourteen representative samples encompassing all three types of hydrothermal precipitates (mounds, active and inactive spires) were selected for bulk chemical analysis. The 50-g samples were ground by hand in an agate mortar or powdered in an alumina mill to <-200 mesh. Silica contamination is estimated to be less than 0.3%. Bulk chemical analyses were done by X-Ray Assay Laboratories Ltd. of Don Mills, Ontario, and involved a wide variety of techniques including X-ray fluorescence spectrometry, argon-plasma-emission spectrometry, flameless and graphite furnace atomic absorption, neutron activation, fire assay, and wet chemistry. Additional analyses performed at the University of Toronto were done by instrumental neutron activation (INAA).

Because of their friable nature, samples selected for fluid-inclusion study had to be impregnated with a slurry of fine-grained portland cement and water under vacuum. Doubly-polished thin sections, 60 to 100 μm thick, were prepared from the impregnated specimens (following the method of Holland *et al.* 1978). A Linkam TH600 programmable heating-cooling stage (Shepherd 1981) was used to make microthermometric measurements. Repeated calibration utilizing the known melting points of various substances (McDonald & Spooner 1981) within the temperature range of interest were performed prior to and during microthermometric work to correct for drift. In order to overcome problems associated with stretching of fluid inclusions during homogenization runs, inclusion sections were broken into many smaller chips. All freezing work was done prior to heating, and each chip was heated only once.

Descriptive and Chemical Mineralogy

Samples for mineralogical study were selected to encompass all deposit morphologies and to cover a large areal extent. Table 1 lists the minerals identified and their abundances. All analyses cited below are by electron microprobe.

Sulfides

Pyrrhotite. Pyrrhotite is ubiquitous in all samples as thin euhedral hexagonal plates from <0.01 to 2.5 mm across (Figs. 5a,b). Plates radiate perpendicularly from growth surfaces into open spaces or cavities. Where cavities are absent, pyrrhotite plates are intergrown in a random or boxwork fashion. Plates are incipiently fractured and, in inactive spires and certain mound samples, are partly to completely oxidized to lepidocrocite and crusts of goethite and amorphous iron oxyhydroxide. Pyrrhotite plates also form coalescent aggregates and microcrystalline inclusions in other minerals such as anhydrite and calcite. The inclusions delineate growth zones and are indicative of fluctuating physicochemical conditions of the hydrothermal fluid from which the minerals were precipitated. Analyses indicate that the pyrrhotite contains only Fe and S. The mole fraction of FeS in pyrrhotite varies from 0.933 to 0.960 (mean = 0.947, 1σ = 0.008, N = 19). XRD patterns identified only so-called "hexagonal" pyrrhotite (Kissin & Scott 1982). No attempt was made to identify polytypes. Pyrrhotite in the Guaymas Basin deposits is stabilized relative to FeS_2 by the low aO_2 of the discharging reduced vent fluids (Scott 1985).

TABLE 1. COMPARATIVE MINERALOGY OF GUAYMAS BASIN SAMPLES

MINERAL	IDEAL FORMULA	MOUND	INACTIVE CHIMNEY/SPIRE	ACTIVE CHIMNEY/SPIRE
pyrrhotite	$Fe_{1-x}S$	XX	X	XX
marcasite	FeS_2	- to XXX	-	-
pyrite	FeS_2	XX	-	-
sphalerite	(Zn,Fe)S	X	X	XX
wurtzite	(Zn,Fe)S	-	X	XX
galena	PbS	X	X	X
isocubanite	$CuFe_2S_3$	X	X	XX
chalcopyrite	$CuFeS_2$	-	X	X
anhydrite	$CaSO_4$	- to XX	X	XXX
barite	$BaSO_4$	XXX	XXX	XXX
calcite	$CaCO_3$	XXXX	XXXX	XXXX
aragonite	$CaCO_3$	-	-	X
amorphous silica	SiO_2	XXXX	XXXX	XX to XXX
stevensite	Mg-smectite	- to XXXX	-	- to XXX
clay		- to XXXX	-	-
iron oxides		XX	X	-

XXXX abundant, XXX moderate, XX minor, X trace, - absent.

Marcasite and pyrite. Secondary marcasite, which may have formed stably (Murowchick & Barnes 1986), is common in many mound samples as pseudomorphs of pyrrhotite, anhydrite, and amorphous silica (Fig. 5c). Colloform and framboidal marcasite were not observed. Pyrite is only a minor constituent within crusts of lithified sediments from the exterior of mounds, where it occurs as colloform spheres, possibly oolitic, averaging 0.01 mm in diameter (Fig. 5d), finely-dispersed framboids 0.01 to 0.4 mm in diameter (Fig. 5d), anhedral to subhedral blebs, and rarely as euhedral cubes. Pyrite is conspicuously absent in spires. Framboidal pyrite consists of spheroidal aggregates of submicrometer particles, whereas pyrite spheres contain colloform growth layers.

Sphalerite and wurtzite. Other than pyrrhotite, zinc sulfide is the most common sulfide. Both sphalerite and wurtzite are present in all sample types, but generally cannot be distinguished by microscopy because high iron contents render most crystals opaque. The general term zinc sulfide is used wherever distinction is not possible, although sphalerite is estimated to predominate by far over wurtzite.

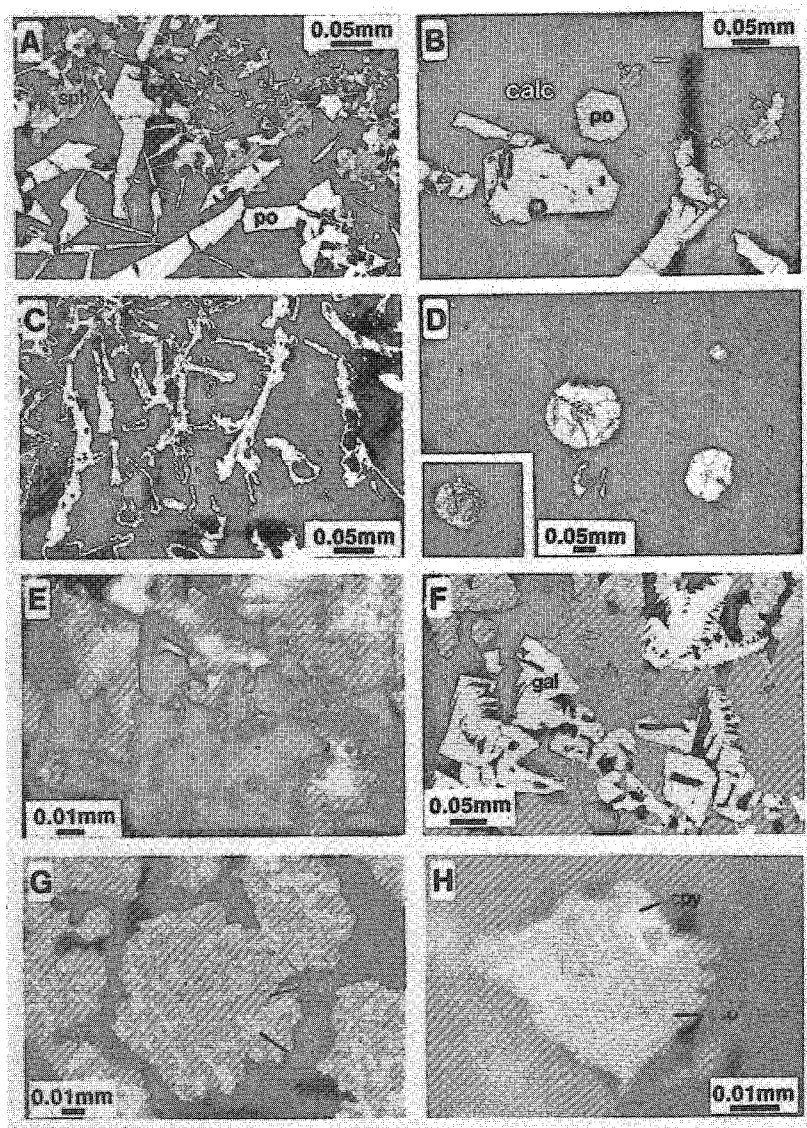

FIG. 5. Sulfide textures. A) Boxwork intergrowth of pyrrhotite plates (po) with minor sphalerite (sph) in calcite (calc) (sample 1173-15, reflected light). B) Hexagonal pyrrhotite plate (po) in calcite (calc). A smaller bleb of intergrown sphalerite–isocubanite and galena is at the right (sample 1174-4, reflected light). C) Marcasite pseudomorphs of pyrrhotite plates in calcite (sample 1175-8, reflected light). D) Colloform spheres and framboids (inset) of pyrite in lithified mound sediment (sample 1175-8, reflected light). E) Hexagonal wurtzite crystals in calcite (sample 1173-1, plane-polarized transmitted light). F) Skeletal galena in sphalerite with intergrowths of isocubanite and sphalerite at top left (sample 1173-6, reflected light). G) Vermicular intergrowth of sphalerite (sph) and isocubanite (iso) (sample 1173-6, reflected light). H) Crystallographically oriented exsolution lenses of chalcopyrite (cpy) in isocubanite (iso) (sample 1173-6, reflected light).

Wurtzite was identified by its hexagonal crystal habit, anisotropy in transmitted light (Fig. 5e), and its XRD pattern. No color zoning is present. Crystals are prisms 0.01 to 0.1 mm in diameter. Sphalerite and wurtzite have different stoichiometries, and the phase transition is a function of T and aS_2 (Scott &

Barnes 1972). Scott & Barnes (1972) placed the transition from sphalerite to wurtzite at low aS_2 values, within the pyrrhotite stability field at $T > 150°C$. Wurtzite is thought to be unstable relative to sphalerite in inactive chimneys and mounds (Zierenberg *et al.* 1984). Active spires at Guaymas Basin contain fluid at higher T and lower aS_2 than mounds and inactive spires. Consequently, wurtzite is expected to occur mainly in active spires, and sphalerite to predominate in inactive spires and mounds. Indeed, wurtzite is generally observed only in the inner walls and undersides of eaves of active vents. XRD patterns of hexagonal-shaped zinc sulfide crystals from inactive spire samples revealed only sphalerite. Wurtzite crystals commonly contain numerous minute inclusions of isocubanite. These inclusions are so small and dispersed that the optical properties of wurtzite are altered in reflected light. Locally, wurtzite is replaced by isocubanite, galena, or both.

Sphalerite occurs as anhedral grains, <0.01 to 0.2 mm in diameter (Figs. 5a,f), that were deposited on, and locally replaced, pyrrhotite plates. In most samples, sphalerite is associated with isocubanite and galena, with which it displays mutually interpenetrating boundaries. Sphalerite also commonly occurs as arborescent and plumose intergrowths with isocubanite (Fig. 5g). In mound and inactive spire samples, sphalerite has been partly oxidized to iron oxide along rims and in fracture fillings.

Cu in most samples ranges from 0 to 0.9 wt.%, but is generally absent (mean = 0.1, 1σ = 0.2, N = 44). Several higher values (2.3 to 9.9 wt.%, N = 8) probably reflect fine-grained isocubanite inclusions. Mn contents range from about 0.2 to 4.4 wt.% (mean = 1.5, 1σ = 1.4, N = 52) and are quite variable among samples. Mn presence is consistent with solubility calculations of Bowers *et al.* (1985) which indicate that Guaymas Basin hydrothermal solutions are saturated with respect to alabandite (MnS). Cd contents are below the minimum detection limit (MDL) of about 0.1 wt.%. Fe contents of sphalerite and wurtzite are among the highest found in nature, generally ranging between 25 and 44 mole % FeS (Fig. 6), but some are as high as 50–55 mole %. Only one of these latter analyses has concomitant high Cu, possibly from a subsurface inclusion of isocubanite. The implied range in aS_2 estimated from the FeS content of zinc sulfide coexisting with pyrrhotite (Scott & Barnes 1971, Hutchison & Scott 1983) is 10^{-12} to 10^{-23}, and is probably symptomatic of strongly fluctuating or disequilibrium conditions.

Microprobe traverses across single crystals reveal complex compositional zoning not evident by optical microscopy because of crystal opacity. Such zoning is expected because the aS_2 is unlikely to be buffered so precisely as to give constant iron contents. Fe concentration in zinc sulfide is also very temperature-sensitive (Scott & Barnes 1971), and temperature fluctuations in the hydrothermal fluid could equally explain the spread of the data in Figure 6.

Isocubanite. Isocubanite's composition lies in the central portion of the Cu–Fe–S system (*e.g.,* Mikaiyama & Isawa 1970, Cabri 1973, Cabri *et al.* 1973, Craig & Scott 1974, Sugaki *et al.* 1975, Wiggins & Craig 1980). Isocubanite is present in trace amounts in almost all samples, and is a minor constituent in several spire samples. It occurs as anhedral blebs, as plumose and arborescent intergrowths with sphalerite (Fig. 5g) which probably result from epitaxial precipitation of isocubanite on wurtzite, as replacements of pyrrhotite and zinc sulfide along fractures, and as numerous inclusions of <1 μm in zinc sulfide ("chalcopyrite disease" of Barton 1978 and Barton & Bethke 1987). Microprobe-detected

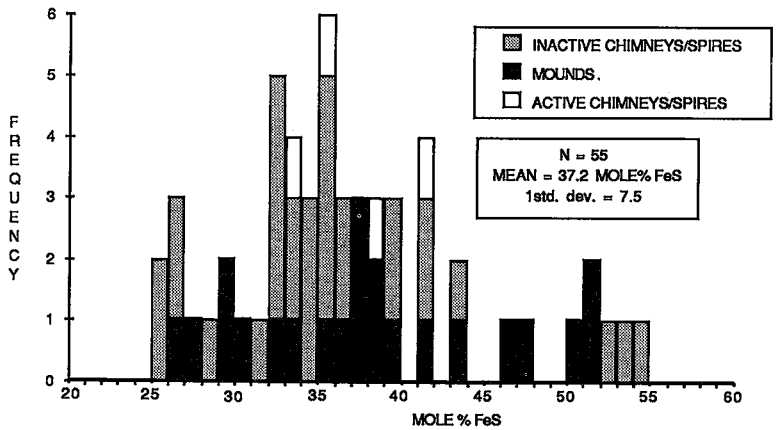

FIG. 6. Histogram of mole % FeS in zinc sulfide from Guaymas Basin.

minor elements in isocubanite are Zn (mean = 2.3 wt.%, 1σ = 1.4, N = 32) and Mn (mean = 0.2 wt.%, 1σ = 0.1, N = 10).

The anhedral blebs of isocubanite commonly contain crystallographically oriented lensoid exsolution lamellae of chalcopyrite (Fig. 5h). The lamellae result from the breakdown of an initial phase to chalcopyrite and isocubanite during rapid cooling (Cabri 1973). Quenching from >210°C preserves the cubic form of isocubanite. Chalcopyrite also rims and replaces isocubanite in some samples, penetrating the mineral in irregular fracture fillings or along its crystallographic axes (Fig. 5h).

Galena. Galena is present in trace amounts in all sample types, and in some chimneys it comprises up to 5 vol.%. Grain size varies from <0.1 to 0.2 mm. Galena occurs as anhedral grains to subhedral crystals, as rare euhedral cubes within pyrrhotite, as crystals on pyrrhotite, and as a replacement of pyrrhotite. Galena displays mutual boundaries with sphalerite, and locally replaced or filled fractures in it. Atoll structures derived by selective replacement by calcite (Fig. 5f) are also present. Although chemical analyses of bulk samples indicate the presence of Ag, no Ag in galena was detected in EDX spectra. Koski *et al.* (1985) examined dredged mound material and also failed to identify a silver-bearing phase. They appealed to the presence of a Pb–As sulfosalt to explain the high Ag values.

Sulfates

Anhydrite. Anhydrite, intergrown with barite, is

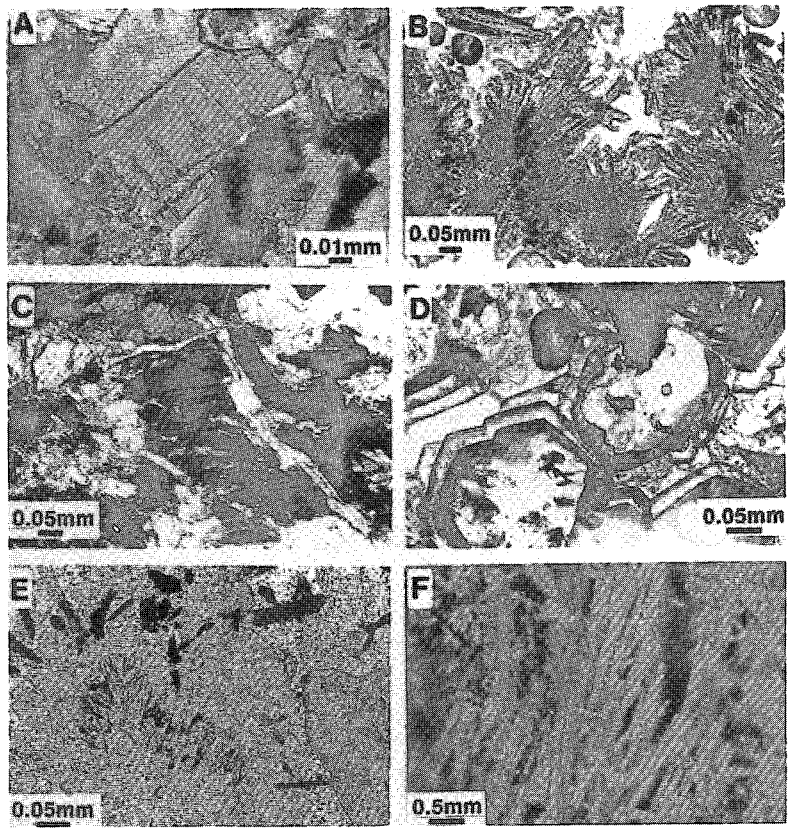

FIG. 7. Mineral textures of non-sulfide phases. A) Tabular anhydrite crystal. A planar array of fluid inclusions defines a growth zone (sample 1173-5, plane-polarized transmitted light). B) Network of radiating acicular barite crystals (sample 1175-7, plane-polarized transmitted light). C) Veinlets and patches of calcite (white) that cross-cut and replace earlier calcite (dark grey) (sample 1174-4, cross-polarized transmitted light). D) Growth-zoned calcite crystals (sample 1169-1B, plane-polarized transmitted light). E) Fine-grained pyrrhotite inclusions defining growth zones in calcite (sample 1174-7, cross-polarized transmitted light). F) Bundles of stevensite fibers intergrown with pyrrhotite (sample 1174-8A, incident light).

predominantly in active spire and mound samples and is absent, or is present only in trace amounts, in inactive spires. This observation is consistent with the retrograde solubility of anhydrite, whereby anhydrite precipitated at >140°C in seawater is redissolved at lower temperatures (Blount & Dickson 1969). Anhydrite occurs as aggregates of radiating acicular crystals, 0.5 mm long, and as elongate tabular crystals 0.2 to 0.3 mm long (Fig. 7a). It commonly contains fine-grained sulfide inclusions which delineate growth zones, but some anhydrite is inclusion-free. Typically, cores of anhydrite are clouded with inclusions, and rims are clear. Many acicular anhydrite crystals are partly to completely pseudomorphosed by fine-grained calcite.

Barite. Barite is present in trace to major amounts in all sample types, and some inactive spires and mounds contain up to 30 vol.%. Barite occurs predominantly in the outer portions of spires as small, tabular, euhedral crystals with wedge-like terminations. Crystals are <0.01 to 0.3 mm and average 0.2 mm in length. Rarely, large anhedral barite grains poikilitically enclose slender prisms of anhydrite and rhombs of calcite. In many samples barite has formed after anhydrite and sulfides, occurring in cavities as clusters of small needle-like crystals perpendicular to the substrate (Fig. 7b). Sr is ubiquitous in minor amounts (mean = 1.2 wt.%, 1σ = 0.6, N = 7), and Ca was found in only one sample (0.2 wt.%). No other elements were detected.

As pointed out by Koski *et al.* (1985), the presence of barite and anhydrite as intergrowths with pyrrhotite in some chimneys must represent a disequilibrium assemblage. They should, however, precipitate upon mixing of the vent fluids with sulfate-enriched seawater. Sulfur isotope analyses of Guaymas Basin barite and anhydrite range from 20.7 to 26.4‰, and indicate that the source of sulfur in these minerals is seawater sulfate that has been reduced in the vent fluid or source area (Peter *et al.* 1986). For barite from Guaymas Basin dredge samples, Koski *et al.* (1985) obtained temperatures of formation of 208 and 215°C from oxygen isotopic analyses. These are 80 to 100°C lower than temperatures determined from fluid inclusions in calcite which accompanied sulfide deposition (see below), and must reflect mixing of hydrothermal fluid with cold seawater.

Carbonates

Calcite is very abundant in spires, approaching 100 vol.% in some samples, but is not common in mound samples. It is a principal constructional component of spires; crystals typically line orifices and have their long axes normal to the direction of fluid flow. Calcite displays two habits: 1) anhedral grains to subhedral interlocking crystals 0.01 to 3.0 mm in diameter, and 2) acicular and commonly radiating crystals 0.5 to 0.8 mm by 0.05 mm which are pseudomorphs of anhydrite. Some crystals of type-1 contain dendritic sulfide inclusions or poikilitically enclose discrete pyrrhotite plates (Fig. 7e). Type-2 crystals invariably contain disseminated fine-grained sulfide inclusions which locally envelope the pseudomorph. The numerous sulfide inclusions impart a cloudy, dark grey-brown color to the crystals. Most calcite pseudomorphs appear to be an agglomeration of smaller calcite grains, although a few pseudomorphs are optically continous and appear to be single crystals. The small crystallite size of the agglomerations is presumably due to rapid chemical replacement. Calcite commonly displays growth zoning (Fig. 7d), with individual zones defined by planar arrays of extremely fine-grained pyrrhotite inclusions. Such zoning indicates a dynamic change in vent-fluid chemistry or physical parameters (or both) during mineral precipitation. Rarely, calcite crystals are dissected by veinlets of calcite (Fig. 7c). Precipitation of calcite could result either from a decrease in temperature by mixing with seawater, or by degassing of CO_2 from the vent fluid. Considering the high CO_2 content of the vent fluids (Von Damm *et al.* 1985) and the retrograde solubility of calcite (Ellis 1963), the latter mechanism seems more likely.

Partial microprobe analyses of calcite gave 0.3 to 2.8% Mn (mean = 1.4 wt.%, 1σ = 0.9, N = 7), and Fe from <MDL to 0.2 wt.% (mean = 0.04 wt.%. 1σ = 0.07, N = 7). Mg was not detected. Cathode luminescence showed no compositional zoning but did produce a bright red-orange color indicative of Mn (Nickel 1978). For calcite from chimneys, $\delta^{13}C_{pdb}$ ranges from −9.6 to −14 (N = 40; Peter *et al.* 1986). This suggests that CO_2 in the vent fluids was derived mainly by mixing equal amounts of carbon from two sources: oxidized organic matter, and dissolved marine carbonate. Aragonite is a rare constituent of spires and has not been found in mound samples. Crystals are typically corroded or embayed. Aragonite's rarity is explained by its transformation to calcite in the presence of seawater (*e.g.*, Cooke & Kepkay 1980a,b).

Silicates

Stevensite. Several greyish to drab olive-green samples from mounds (*e.g.*, 1170-5) contain a mineral whose colloform habit is suggestive of deposition from a lower temperature fluid, as is consistent with the lower temperatures within mounds. Another sample, a piece from a chimney actively venting black smoke (1174-8A), contains a fibrous mineral. Individual fibers are extremely delicate, slender (0.1 mm), and typically several cm long. Fibers occur in radiating aggregates intergrown with fine-grained sulfides predominated by pyrrhotite (Fig. 7f).

Samples 1170-5 and 1174-8A are composed predominantly of Mg, Na, and Si. The XRD charac-

teristics of thermally treated and glycolated samples, together with chemical analyses, correspond to stevensite (Brindley 1980, Brindley *et al.* 1977), a trioctahedral 2:1 smectite with the ideal formula $Na_{0.33}Mg_{2.83}Si_4O_{10}(OH)_2$ (Hathaway 1979). Al substitutes for Si in the tetrahedral layer, and Na–Mn substitutes for Mg in the octahedral layer. Possible Fe substitution is uncertain because the samples contain iron sulfide contaminants.

Amorphous silica. Amorphous silica is abundant both in spire and mound samples, though it is present in greater amounts in mounds. The XRD pattern has a diffuse peak at about 3.8–4.1 Å characteristic of opal A (Jones & Segnit 1971, 1975). Silica displays three habits: colloform layers, spheres or globules, and fibers or filaments (Figs. 8a,b,c). Layers of silica approximately 0.02 mm thick can coat all other primary minerals (Fig. 8c). In some places, multiple growth layering is evident. Uniformly-sized silica spheres, 0.03 to 0.1 mm in diameter, occur in clusters (Fig. 8c) which are best trapped and preserved in pores and cavities. The fibers or filaments are about 0.1 mm in diameter (Fig. 8a), are bent, and some are branched. Locally, the fibers coalesce and have a mesh-like appearance. Juniper & Fouquet (1988) have interpreted such structures in other modern

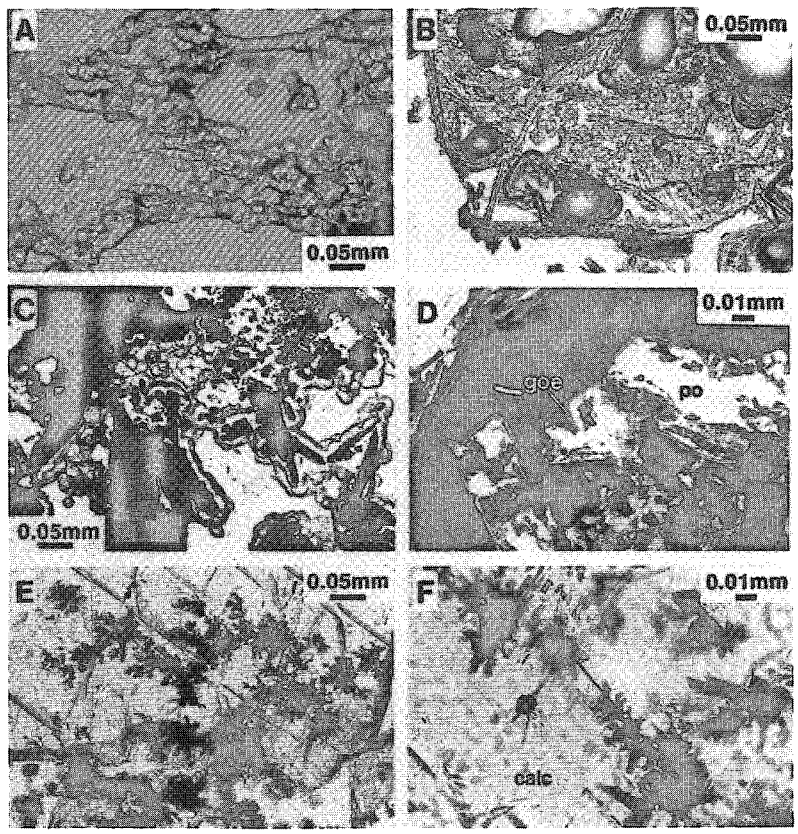

FIG. 8. Amorphous silica, oxidation, and biological textures. A) Rods of amorphous silica composed of smaller silica spheres. This texture results from the coating of filamentous bacteria by amorphous silica (sample 1175-7, plane-polarized transmitted light). B) Calcite crystals pseudomorphed by amorphous silica (sample 1169-1B, plane-polarized transmitted light). C) Amorphous silica spheres which coat pyrrhotite, sphalerite, and isocubanite (sample 1172-2A3, plane-polarized transmitted light). D) Rims of goethite (goe) on pyrrhotite plates (po) (sample 1172-2A3, reflected light). E) Fine-grained sulfides on bacterial filaments included in calcite (sample 1169-1B, plane-polarized transmitted light). F) Close-up of sulfides encrusting bacterial filaments in calcite (calc) (sample 1169-1A1, plane-polarized transmitted light).

seafloor-vent deposits to be branching microbial filaments coated by amorphous silica. The silica is abiogenic and filaments merely serve as a substrate for deposition. Other fibers of silica having no apparent relation to microbial filaments rarely replace anhydrite, barite, calcite, and even worm tubes.

Conductive cooling has been suggested by Janecky & Seyfried (1984) and Tivey & Delaney (1986) as the dominant cause of deposition of amorphous silica a 21°N, Galapagos Rift, and the Endeavor Segment. If the temperature of hydrothermal fluid decreases solely as a consequence of mixing with seawater, the solubility of silica is never exceeded due to the dilution effect (but is approached near 100°C) even if no other silicates such as stevensite have precipitated (Chen & Marshall 1982). Hydrothermal fluid cooling solely by conduction could begin to precipitate amorphous silica at about 250°C, and a combination of conductive cooling and mixing with seawater would result in precipitation below 250°C. Bowers *et al.* (1985) have modelled the conductive cooling of Guaymas Basin vent fluid and concluded that such a process can explain the observed chemistry. Conductive cooling therefore may explain the greater abundance of silica in mounds than in spires.

Biological phases

In addition to the silica fibers interpreted to have formed on filamentous bacterial structures, some samples contain remnants of filamentous bacterial mats; submersible observations have shown that similar mats commonly encrust sulfides at Guaymas Basin. Aggregates of filaments with very fine sulfide crystals precipitated on them are preserved in calcite (Figs. 8e,f). Single filaments are 0.5 to 1 μm in diameter and up to 150 μm long. That these were entrapped at >200°C is indicated from fluid-inclusion data from the surrounding calcite. Well-preserved filaments are rare, but biogenic material clearly has played an important role in the mineralizing process by serving as a substrate for silica–sulfide deposition.

Mineral distribution

Table 1 compares the mineralogy of the different sample types. There are distinct differences between spire and mound samples, and even between active and inactive spires: marcasite is present only in mounds, wurtzite and chalcopyrite are present only in spires, anhydrite is generally absent in mounds, aragonite is present only in active spires, and amorphous silica and barite are far more abundant in mounds than in spires.

Zonation of most of the spire samples is poor or absent, probably because the many small anastomosing hydrothermal discharge pathways precluded any consistent thermal gradient. The few chimneys that do display concentric mineralogical zoning about their orifice (Figs. 4a,b) have a core of massive chalcopyrite/isocubanite surrounded by a massive zinc sulfide ± galena annulus, an exterior zone of disseminated zinc sulfide in a calcite–sulfate matrix, and

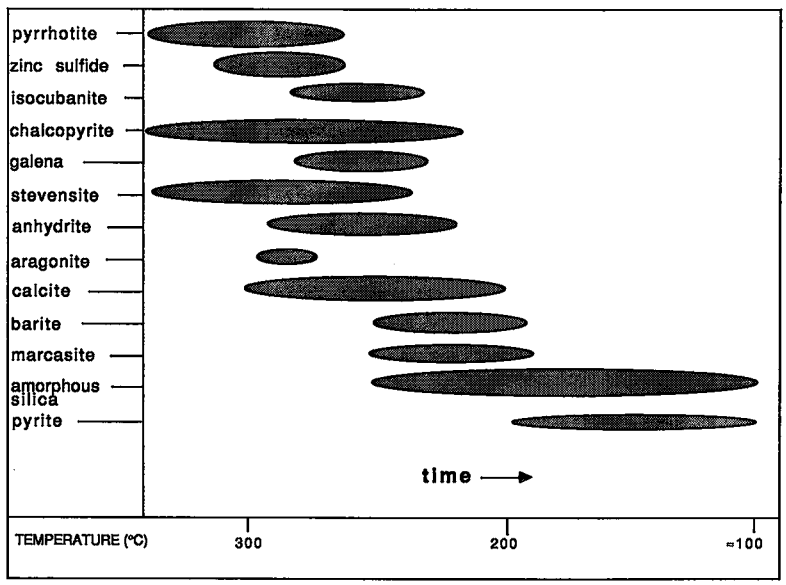

FIG. 9. Generalized paragenetic sequence of mineralization in Guaymas Basin samples.

TABLE 2. DESCRIPTION AND MINERALOGY OF SAMPLES SELECTED FOR BULK CHEMICAL ANALYSIS AND FLUID INCLUSION MICROTHERMOMETRY

SAMPLE	DESCRIPTION	MINERALOGY
1168-2	from mildly active (0-50°C) mound, tan to light grey aggregate of white crystals and clay; well indurated.	sph, iso, py, clay, diatom debris, iron oxide.
1169-1A1	basal cross section of an 80 cm tall inactive chimney; light grey.	po, py, sph, iso, gal, amorphous silica, anhy, barite.
1169-1B	mid-section of an 80 cm tall chimney.	calc, amorphous silica, anhy, barite, po, ZnS, iso, gal, aragonite, barite.
1170-3	≈15 cm tall active spire with a mushroom-shaped eave. 273°C fluid vented from underside of eave.	calc, anhy, po, ZnS, iso, py, gal, aragonite, barite.
1170-5	inactive (?) mound; medium green-brown; very friable.	sample rich in clay and stevensite.
1170-10	cross-section of small 15 cm tall inactive spire without central orifice, but many smaller holes; grey to black.	po, sph, iso, gal, cpy, calc, anhy, amorphous silica, barite.
1170-19	cross-section of an inactive spire; no central orifice, but many smaller holes; sulfide-rich; dark grey to black.	po, sph, gal, cpy, barite, calc, amorphous silica.
1170-24	inactive (?) mound; medium brown.	po, sph, barite, amorphous silica, clay.
1172-2	composite sample of an 85 cm tall inactive spire; no central orifice, but many smaller holes; sulfide-rich; grey to black.	po, sph, cpy, iso, gal, calc, barite, anhy, amorphous silica.
1172-3	inactive (?) mound; greenish.	po, sph, barite, stevensite.
1173-1	piece of eave from spire actively venting 291°C fluid from the underside of the eave.	calc, po, barite, anhy, ZnS, iso, gal.
1173-6	small, 7 cm diameter inactive chimney; 2 cm diameter orifice.	calc, ZnS, gal, po, iso, cpy, iron oxide.
1173-14	cross-section of an eave of a 17 m tall spire venting 291°C fluid from under the eave; high specific gravity.	po, sph, gal, iso, py, calc, barite, anhy, amorphous silica.
1174-3	cross-section taken about half way up a 50 cm tall inactive spire; well indurated, creamy white, fine-grained sample with red and orange staining.	po, sph, iso, barite, anhy, amorphous silica, iron oxide.
1174-8A	2 m tall spire with eaves actively venting black smoke (temp. unknown); dense aggregate of bundles of acicular green-grey crystals intergrown with minor pyrrhotite.	stevensite, po.
1175-8	mound with a crust of orange-brown iron oxide; high specific gravity.	po, py, iso, sph, marcasite, barite, anhy, amorphous silica.
1175-10	small chimney with pyrrhotite-lined orifice.	calc, amorphous silica, po, ZnS, iso, gal, py, iron oxide.
1177-1	spire actively venting 312°C fluid from a central orifice; very dense, high specific gravity; creamy white with orange brown staining on surface.	po, sph, iso, barite, anhy, amorphous silica, iron oxide.
1177-6	mound with iron oxide crust.	po, sph, iso, calc, barite, amorphous silica.

Mineral abbreviations: sph sphalerite, iso isocubanite, py pyrite, po pyrrhotite, gal galena, anhy anhydrite, ZnS zinc sulfide, calc calcite, cpy chalcopyrite.

TABLE 3. BULK CHEMICAL ANALYSES OF GUAYMAS BASIN SAMPLES

ELEMENT	SAMPLE NUMBER													
(wt.%)	1168-2	1169-1A1	1170-5	1170-10	1170-19	1170-24	1172-2	1172-3	1173-14	1174-3	1174-8A	1175-8	1177-1	1177-6
Fe	0.3	1.32	2.22	31.8	12.59	1.62	4.03	0.34	4.54	0.55	3.99	12.8	3.78	2.10
Zn	0.0023	0.23	0.86	3.78	1.58	0.32	0.58	0.26	0.81	0.02	2.89	0.43	1.69	0.062
Cu	0.00055	0.06	0.28	0.43	0.23	0.05	0.08	0.05	0.19	0.03	0.42	0.16	0.44	0.015
Pb	0.00060	0.13	0.4	2.13	0.91	0.05	0.26	0.03	0.62	0.01	0.02	0.47	0.05	0.0028
S	NA	3.71	0.84	NA	8.82	0.93	5.70	0.57	3.53	0.19	0.1	NA	5.10	NA
SO3	NA	0.41	0.10	NA	3.78	8.37	5.70	10.83	1.51	9.09	11.10	NA	5.10	NA
BaO	0.001	11.5	1.80	0.09	13.3	35.4	37.9	48.8	2.13	42.4	0.36	11.6	0.49	27.2
SiO2	81.0	31.1	50.0	32.5	34.6	25.7	2.72	5.94	6.78	30.0	20.5	41.4	5.91	29.8
Al2O3	7.18	0.11	3.12	NA	0.28	1.09	0.26	0.79	0.02	0.49	0.87	0.28	0.11	5.20
CaO	0.33	24.2	0.05	0.14	7.0	0	13.5	0	37.6	0.039	15.8	0.15	32.9	0.50
MgO	1.48	0.61	26.39	NA	0.12	1.49	0.32	2.57	0.20	0.13	10.2	0.55	1.38	9.70
NaCl	NA	1.17	2.31	NA	1.37	1.35	1.14	0.99	0.64	0.84	2.08	NA	0.43	NA
KCl	NA	0.23	0.34	NA	0.13	0.32	0.04	0.15	<0.02	0.13	0.40	0.11	0.02	NA
Sr	NA	0.438	0.054	NA	0.305	0.577	0.120	0.561	0.120	0.517	0.110	NA	0.120	NA
Mn	NA	0.50	0.11	0.18	0.41	0.02	0.70	0.008	0.88	0.02	0.13	0.01	0.38	0.03
TiO2	NA	0.10	0.13	NA	0.08	0.20	0.18	0.23	0.01	0.22	<0.01	NA	<0.01	NA
P2O5	NA	0.02	0.11	NA	0.02	0.05	0.02	0.03	0.02	0.05	0.02	NA	0.02	NA
CO2	0.1	17.5	0.3	1.1	5.0	3.0	11.0	0.1	30.6	0.3	3.4	0.2	21.8	0.2
LOI	NA	5.39	14.6	NA	18.1	19.2	-1.46	12.5	16.4	2.08	24	NA	22.1	NA
TOTAL	—	98.73	104.0	—	108.63	99.74	82.79	84.75	106.60	87.14	96.39	—	101.82	—
(ppm)														
Ag	<0.5	16.8	19.5	28.5	353.2	205.4	126.2	53.8	15.1	47.7	TRACE	97.4	4.1	3.0
As	NA	67.0	24.0	NA	280.0	110	67.0	38.0	280.0	240.0	40.0	NA	240.0	NA
Au	NA	0.046	0.1	NA	0.220	0.270	0.035	0.093	0.350	0.160	0.041	NA	0.140	NA
Bi	NA	0.6	0.1	NA	2.9	0.1	0.3	<0.1	1.7	<0.1	9.9	NA	8.2	NA
Cd	<1	4	41	<1	67	20	29	19	24	2	110	22	58	4
Co	4	NA	NA	4	NA	NA	NA	NA	NA	NA	NA	3	NA	8
Cr	NA	<10	<10	NA	<10	<10	<10	<10	<10	<10	<10	NA	<10	NA
Ge	NA	<10	<10	NA	<10	<10	10	<10	20	<10	<10	NA	<10	NA
Mo	1.0	NA	6	11	NA	19	NA	29	NA	4	<1	17	<1	30
Nb	NA	20	20	NA	10	10	<10	<10	10	<10	10	NA	20	NA
Ni	9	NA	NA	9	NA	NA	NA	NA	NA	NA	NA	44	NA	47
Rb	NA	<10	<10	NA	<10	<10	<10	<10	<10	<10	<10	NA	<10	NA
Sb	NA	17.0	140.0	NA	490	NA	140	NA	40.0	38.0	4.6	NA	18.0	NA
Se	NA	30.0	75.0	NA	250	730	110	590	120	9.0	85.0	NA	80.0	NA
Sn	NA	<3	3	0	12	3	<3	<3	3	3.0	3	0	3	NA
Te	NA	4.2	0.2	NA	0.2	0.3	0.2	0.1	5.2	1.1	1.8	NA	2.1	NA
U	NA	3.2	NA	NA	2.6	NA	1.2	NA	0.4	NA	NA	NA	NA	NA
Y	NA	<10	<10	NA	<10	<10	<10	<10	<10	<10	<10	NA	<10	NA
Zr	NA	50	20	NA	80	280	<10	280	<10	260	30	NA	40	NA

NA = not analyzed

Concentrations of Si, Al, Ca, Mg, Na, K, Fe, Mn, Ti, P along with Sr, Rb, Cr, Y, Nb, and Zr were determined by wavelength-dipersion X-ray fluorescence spectrometry on fused glass discs (detection limits of 0.01 wt % and 10 ppm, respectively). Concentrations of Fe, Zn, Cu, Pb, Ag, Cd, Co, Ge, Mo, Mn, and Ni in the ppm range were determined by multi-element direct coupled argon plasma-emission spectrometry (detection limits of 1.0 ppm). CO_2 was analyzed by wet-chemical methods. As, Sb, and Bi were determined by flameless atomic absorption utilizing a heated quartz tube furnace, and Te and Se by graphite-furnace atomic absorption (detection limits of 0.1 ppm). U was measured by INAA. Ag was determined by fire assay (detection limits of 0.5 ppm). Au was analyzed by fire-assay preconcentration followed by direct coupled plasma-emission spectrometry (detection limit, 2 ppb).

an outer rim of calcite ± anhydrite ± barite. Similar zonation (without calcite) has been observed in chimneys recovered from other hydrothermal vent sites (*e.g.*, Oudin 1983, Haymon 1983). Certain chimneys display multiple episodes of such zoning, or have a layer of calcite lining the chalcopyrite/isocubanite zone. Figure 9 depicts the paragenetic sequence determined from mineral textures.

Bulk Compositions

Locations of the analyzed samples are given in Figure 2, descriptions are in Table 2, and bulk chemical analyses are in Table 3. Totals are not all near 100%. LOI values may not be accurate as they were determined by igniting the samples in air. High values result from oxidation of metals, and loss of S and volatiles such as H_2O, SO_4, and CO_2 during fusion. Redistribution of S values between sulfide and sulfate may also have led to inaccurate totals as original results, given as total S, were divided between sulfide and sulfate based on relative proportions of those minerals estimated by optical microscopy and Ba and Ca analyses. Ba-rich samples (1172-2, 1172-3, and 1174-3) gave particularly low totals. Ba determined by both XRF and INAA gave similar results, so the SO_3 determinations must be too low. Na, K and Cl analyses are reported as salts as all Na and K can be accounted for with an appropriate amount of Cl (except for those samples containing steven-

site). The presence of these salts in the samples cannot be avoided, as washing prior to analysis would dissolve anhydrite.

In general, spires have significantly higher contents of Fe, Zn, Pb, Cu, S, Ca, CO_2, Ag, As, Bi, Cd, Mn, Sn, and Te than do mounds, consistent with the observation that mounds are partly constructed from oxidized chimney talus and debris. The mounds have lower metal contents because they are formed at lower temperatures and thus are dominated by non-sulfide minerals (discussed below). The lower sulfur content of mounds reflects the fact that metal sulfides in mounds are commonly oxidized. As well, anhydrite is dissolved in spire fragments, and this is reflected in the lower Ca values for mounds. Mound samples are higher in both Ba and Si than chimneys and spires, in agreement with barite and amorphous silica being paragenetically late and low-temperature phases.

Fluid Inclusions

Petrology

Petrology and microthermometry of aqueous inclusions were done for samples of six chimneys (both active and inactive) from different locations within the Southern Trough. Inclusions occur in all translucent minerals, but because calcite contains by far the most inclusions and is the dominant mineral intimately associated with sulfides in most spires, it is the focus of this study. The opacity of zinc sulfide precluded the study of fluid inclusions in this material. Anhydrite was not studied because Le Bel & Oudin (1982) found that inclusions in this host give artificially elevated salinities due to partial dissolution of the inclusion walls on freezing. Inclusions in barite were avoided because of their susceptibility to stretching during heating runs (Bodnar & Bethke 1984). Inclusions in amorphous silica are relatively scarce, and this host is not related temporally to sulfide precipitation.

Inclusions were classified as primary or secondary according to the criteria of Roedder (1984). The distinction between secondary and pseudosecondary inclusions was difficult, but given the geologically "instantaneous" growth of a chimney, inclusions classed here as secondary are likely pseudosecondary. Primary aqueous inclusions are 1 to >50 μm, and have a wide variety of cross-sectional shapes. The inclusions are two-phase (aqueous fluid and a vapor bubble), contain no daughter minerals, and typically have uniform phase ratios with the vapor bubble comprising 5 to 20 vol.% of the inclusion (Fig. 10a). On this basis the inclusion fluids do not appear to have undergone phase separation. Primary inclusions are interpreted to contain the extant hydrothermal fluid during mineral growth. Aqueous inclusions are accompanied by liquid and gaseous hydrocarbon-bearing inclusions in certain samples. These inclusions are interpreted to have formed from hydrocarbon that was carried in the hydrothermal fluid as an immiscible phase, and possibly as solvated forms (Peter *et al.* 1988, Peter & Scott 1987).

Welhan & Craig (1982) have measured high concentrations of hydrocarbon (including thermogenic methane) and Von Damm *et al.* (1985) have measured appreciable amounts of H_2S in Guaymas Basin vent fluids. Although CH_4 and H_2S therefore were anticipated in the fluid inlcusions, none was detected.

Secondary inclusions, which far outnumber primary ones in all samples, occur as discontinuous planar arrays along fractures and on healed cleavage planes (Fig. 10b). Secondary inclusions are 1 to >70 μm and are typically irregular. Inclusions along cleavages are slender and needle-like (Fig. 10b). Generally, secondary inclusions are two-phase and consist of an aqueous fluid with a vapor bubble. However, they do not always have uniform phase ratios and, in extreme cases, contain only vapor or liquid. This is most likely due to changes after trapping (*e.g.*, necking). Secondary inclusions are interpreted to have formed from hydrothermal fluid

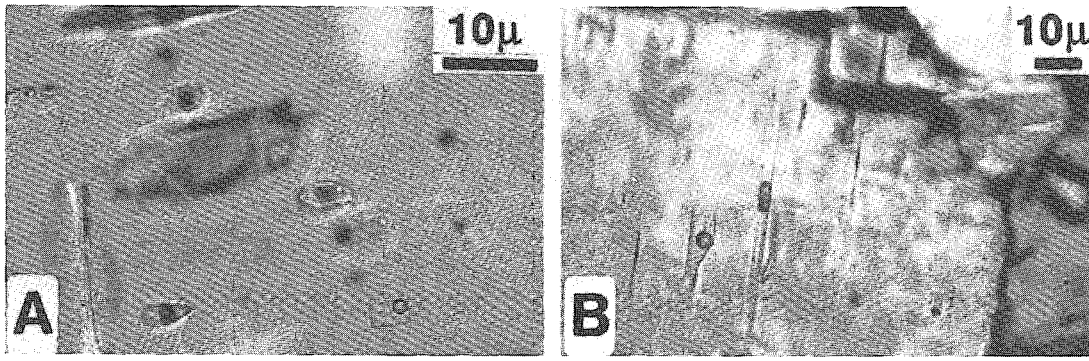

FIG. 10. Photomicrographs of aqueous inclusions. A) Primary, two-phase aqueous inclusions in calcite. B) Elongate, secondary, two-phase aqueous inclusions in calcite.

along fractures during or after late stages of mineral growth.

Microthermometry

Repeated freezing and heating runs on several selected inclusions indicate that freezing temperatures were reproducible to within ±0.5°C, and homogenization temperatures to within ±1 to 4°C. No evidence of clathrate melting was observed.

Some inclusions exhibited eutectic melting of both Na and Ca hydrates. Sudden initiation of melting in most inclusions occurred between −24°C and −19°C, corresponding to the melting of hydrohalite ($NaCl \cdot 2H_2O$). Final melting of ice occurred between −4.6 and −1.3°C. Another cluster of measurements around −49°C corresponds to the eutectic melting of $CaCl_2 \cdot 2H_2O$ (antarcticite). $MgCl_2$ must be negligible in the inclusions as even small amounts lower the eutectic melting point to <52°C (Crawford *et al.* 1979). The hydrohalite melting temperatures allow estimation of the $CaCl_2/NaCl$ ratios in the inclusion fluids. Ratios range from 0 to 0.56:1, with the majority of inclusions giving a ratio of 0.12:1. Table 4 summarizes the results of fluid-inclusion microthermometry for individual chimneys.

Salinities (Fig. 11) were calculated from the temperature of final ice disappearance (freezing point depression) using the equation of Potter *et al.* (1978). The means of primary and secondary fluid-inclusion salinities are 5.3 ($1\sigma = 0.7$) and 5.5 ($1\sigma = 1.1$) equiv. wt.% NaCl, respectively. All measured salinities are higher than Pacific seawater (3.5 equiv. wt.% NaCl), Guaymas Basin vent fluids (3.8 to 4.1% see below), and fluid inclusions from 21°N EPR (3.8% in wurtzite; Styrt *et al.* 1981, 2.9% in anhydrite; Le Bel & Oudin 1982). Salinities are also higher than those obtained by Koski *et al.* (1985) from calcite in Guaymas Basin dredge samples (4.0 to 4.2%). Our values, however, fall within the salinity range of fluid

TABLE 4. SUMMARY OF FLUID INCLUSION MICROTHERMOMETRY DATA

SAMPLE	INCLUSION TYPE	TRAPPING TEMP. (°C)* N	1σ	MEAN	SALINITY (EQUIV. WT. % NaCl) N	1σ	MEAN
1169-1B	primary	30	30.6	213	19	0.49	5.54
	secondary	37	29.7	215	8	0.78	6.43
1170-3	primary	21	17.1	266	16	0.71	5.75
	secondary	29	20.8	229	11	1.2	5.6
1170-15	primary	12	23.1	237	6	0.57	5.05
	secondary	32	33.0	246	5	0.44	4.92
1173-1	primary	1	—	241	1	—	5.3
	secondary	–	—	—	–	—	—
1173-6	primary	29	12.5	277	29	0.52	5.14
	secondary	18	35.5	261	6	0.39	4.95
1175-10	primary	6	21.2	259	5	0.16	4.1
	secondary	8	31.2	235	2	0.21	4.1

*a pressure correction of +15°C corresponding to the 2000m water column overlying the deposits has been added to obtain trapping temperatures for a 5 equiv. wt.% NaCl fluid (Potter 1977).

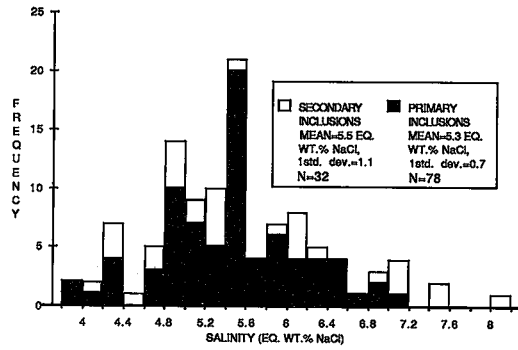

FIG. 11. Frequency distribution of fluid-inclusion salinities for all primary and secondary aqueous two-phase inclusions.

inclusions in some ancient volcanogenic massive sulfide deposits (*e.g.*, 3.5 to 7% in Kuroko deposits: Pisutha-Arnond & Ohmoto 1983, Bryndzia *et al.* 1983, Foley 1986). Elevated salinities have also been reported for inclusions in anhydrite from the southern Juan de Fuca Ridge (about 50% greater than seawater; Brett *et al.* 1985), and from vent fluids of several eastern Pacific sites (Kim *et al.* 1984, Von Damm & Bischoff 1987, Michard *et al.* 1984). Several mechanisms for producing elevated salinities in vent fluids have been proposed (*e.g.*, Bowers *et al.* 1988), but none of these can be tested unambiguously at Guaymas Basin.

Figure 12 gives the frequency distribution of measured homogenization temperatures. A pressure correction (Potter 1977) of +15°C, corresponding to a salinity of 5 equiv. wt.% NaCl and the 2000-m water column overlying the deposits, must be applied to obtain true trapping temperatures. Table 4 lists mean trapping temperatures of populations of inclusions from individual chimneys. The distributions both of primary and secondary fluid inclusions show a pronounced negative skewness of −0.84 and −0.66, respectively, with trapping temperatures as low as 125°C relative to a modal value of 261°C. Such skewed distributions are best explained by the mixing of hot, end-member hydrothermal fluid with cold seawater.

Comparison of microthermometry with fluid chemistry

Fluid-inclusion measurements provide a unique opportunity for comparison with vent-fluid chemical data obtained by Von Damm *et al.* (1985). Fluid-inclusion trapping temperatures (Table 4) are in good agreement with vent-fluid temperatures measured with ALVIN's thermocouple probe. Salinities of vent fluids were calculated from the data of Von Damm *et al.* (1985) using the empirical relation between

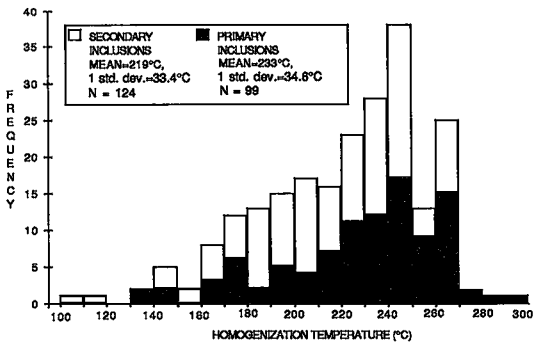

FIG. 12. Frequency distribution of homogenization temperatures for all primary and secondary aqueous inclusions.

salinity (S) and chlorinity (Cl): S (‰) = 0.03 + 1.805 Cl (‰) (Gerrard 1966). Calculated values of salinity range from 3.3 to 4.1 equiv. wt.% NaCl, only slightly above normal seawater values (3.5% NaCl). Enigmatically, with the exception of sample 1175-10 (Table 4), fluid-inclusion salinities are significantly higher than that of seawater and cannot be reconciled with these hydrothermal fluids. The difference is not a result of experimental error.

The end-member fluid chemistry of Von Damm *et al.* (1985) gave calculated values (wt.%) of 3.17 for NaCl, 0.51 for $CaCl_2$, and 0.27 for KCl. $MgCl_2$ is not expected in the fluid inclusions because undiluted vent fluid contains no appreciable Mg (Von Damm *et al.* 1985). The fluid chemistry used in these calculations may not be representative of the fluids trapped in our inclusions, but it can be helpful in assessing melting phenomena observed in fluid inclusions. The fluid chemistry indicates that the cluster of hydrohalite melting measurements betwen −24 and −19°C reflects eutectic melting in the system H_2O–KCl–NaCl at −22.9°C, which is slightly lower than the H_2O–NaCl eutectic at −20.8°C. Such multiple-hydrate melting events are difficult to detect in the inclusions because of the very small volumes of melt generated at the eutectic in low-salinity fluids. The $CaCl_2$/NaCl ratio of 0.16:1 calculated from vent-fluid chemistry data is in good agreement with ratios calculated above from fluid inclusions. Differences between the fluid-inclusion and vent-fluid data such as the salinities, indicate that fluid-inclusion studies of chimney minerals, particularly when paragenetic sequences are known, have considerable potential for delineating complex temporal variations in vent-fluid chemistries.

Mixing of hydrothermal fluid and seawater within chimneys

From the microthermometric data in Table 4 it is apparent that: 1) primary fluid-inclusion homogenization temperatures are higher (by 16 to 37°C) than those for secondary inclusions in three of five samples; and 2) for two of the three samples, primary fluid-inclusion salinities are also concomitantly higher by 0.15 to 0.19 equiv. wt.% NaCl than those for secondary inclusions. In the other samples, salinities of primary and secondary inclusions are indistinguishable. Mann-Whitney U (Mann & Whitney 1947) and Kolmogorov-Smirnov (Siegel 1956) two-tailed, non-parametric tests indicate that homogenization temperatures and salinities obtained from primary and secondary fluid inclusions are from the same population in all the spire samples studied. Differences may arise when cold, ambient seawater (2°C, 3.5 equiv. wt.% NaCl) breaches a chimney wall and enters its interior. The sudden temperature drop may locally fracture the calcite, and the mixture of discharging hydrothermal fluid and ambient seawater along these fractures may become trapped as "secondary" inclusions. The term discharging is used here to describe a fluid immediately at the seawater/seafloor interface (in this case within a chimney, at its base). Such a fluid may have mixed previously with circulating seawater, or a modified component thereof, in the upper zone of the subsurface.

Accompanying this subsurface mixing are changes in temperature, composition (including salinity) and mineral stabilities. If the microthermometric data for primary inclusions accurately reflect the properties of discharging hydrothermal fluid, this fluid has mixed with seawater within individual chimneys in

TABLE 6. HYDROTHERMAL FLUID/SEAWATER MIXING RATIOS CALCULATED FROM FLUID INCLUSION MICROTHERMOMETRIC DATA

SAMPLE	DATA SET	VOLUME % HYDROTHERMAL FLUID	VOLUME % ENTRAINED BOTTOM WATER	MIXING RATIO (HYDROTHERMAL FLUID/SEAWATER)
1169-1B	homog temp*	99	1	99
	salinity	--	--	--
1170-3	homog temp	85	15	5.7
	salinity	92	8	11.5
1170-15	homog temp	--	--	--
	salinity	92	8	11.5
1173-6	homog temp	94	6	15.7
	salinity	90	10	9
1175-10	homog temp	90	10	9
	salinity	100	0	∞

Equations used: $x(Th_1) + (1-x)(T_{sw}) = Th_2$
$x(S_1) + (1-x)(S_{sw}) = S_2$
where x = volume of hydrothermal fluid, (1-x) = volume of ambient seawater, T_{sw} = temperature of ambient seawater in °C (2°C for Guaymas Basin), Th_1 = mean homogenization temperature of primary fluid inclusions, Th_2 = mean homogenization temperature of secondary fluid inclusions in °C, S_{sw} = salinity of ambient seawater in equiv. wt.% NaCl (3.5 eq. wt.% NaCl for Guaymas Basin), S_1 = mean salinity of primary fluid inclusions in eq. wt.% NaCl, and S_2 = mean salinity of secondary fluid inclusions in eq. wt.% NaCl.

*calculated using median value; all others calculated using arithmetic mean values.

--no ratios were calculated; data showed no mixing.

a ratio calculated to be about 9–11.5:1 (Table 5). Not surprisingly, the amount of seawater that has mixed with hydrothermal fluid at the site of mineral precipitation is relatively small.

Sample 1169-1B is the only one in Table 5 which, on the basis of temperature data, displays very little evidence for mixing. The sample is from the midsection of a 0.8-m-high chimney that is taller and has a thicker wall than all other chimneys sampled; consequently, almost no mixing of hydrothermal fluid and seawater would have occurred. Although chimney walls seem to be effective insulators, breaching by cracking, and dissolution by hydrothermal fluids or seawater, must result in some mixing between seawater and hydrothermal fluid (Haymon 1983).

Discussion

A model for the formation of spires and mounds

Figure 13 depicts a model for the growth of spires and mounds. On initiation of venting into ambient seawater, the first minerals to precipitate are anhydrite and stevensite, followed closely by pyrrhotite. The presence of stevensite is consistent with the predicted occurrence of a Mg silicate in Janecky & Seyfried's (1984) mixing model for hydrothermal fluids and seawater. Also, Thornton & Seyfried (1987) found that by reacting an organic-rich, diatomaceous clay from the Gulf of California with seawater at 350°C and 500 bars in an experiment designed to simulate conditions of the Guaymas Basin hydrothermal system, aqueous silica concentrations near amorphous silica saturation developed early and promoted smectite precipitation. Their results suggested that smectite in altered Guaymas Basin sediments and hydrothermal precipitates is more stable than chlorite due to elevated aqueous silica levels associated with the dissolution of diatoms. Bowers *et al.* (1985) calculated that mixing of Guaymas Basin hydrothermal solutions with seawater should result in the precipitation of talc, although the present study indicates that stevensite is the stable Mg silicate. Precipitation of stevensite probably occurs over a large temperature range, as the mineral is found both in mound and active-chimney samples. Guaymas Basin hydrothermal vent fluids are depleted in Mg (Von Damm *et al.* 1985), so Mg in stevensite is likely derived from ambient seawater, whereas the silica probably originates from end-member hydrothermal fluid.

Seawater heated to supersaturation with respect to $CaSO_4$ precipitates anhydrite along with stevensite around the margins of the discharging fluid vent, thereby forming a crust or carapace that is impermeable to seawater (Fig. 13a). Hydrothermal fluid escapes through fractures in this crust, and eventually leads to the formation of juvenile spires. Very young venting structures are composed predominantly of a porous network of minerals, such as anhydrite and stevensite, formed by the mixing of hydrothermal fluid with ambient seawater where a central orifice has not yet formed by mineral dissolution and reprecipitation. Throughout the hot, active life of the chimney or mound, these minerals

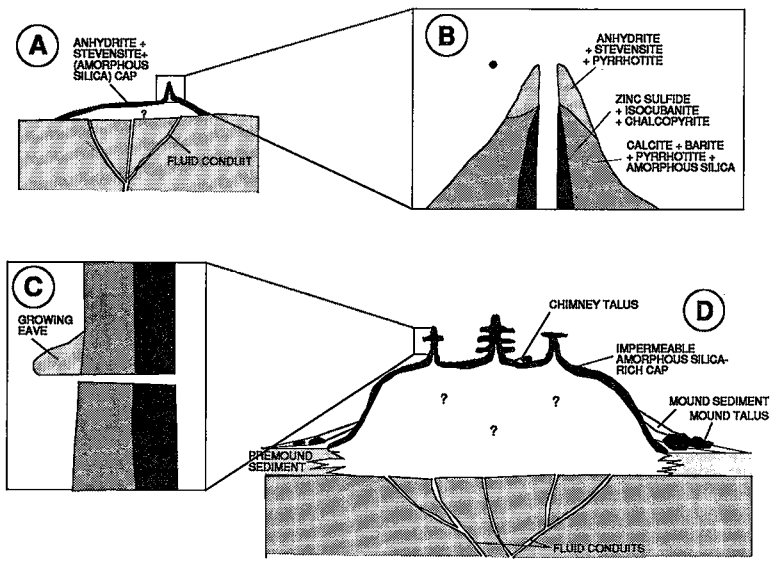

FIG. 13. Generalized development of chimney and mound structures. See text for explanation.

continue to build walls upwards and outwards at the seawater interface (Fig. 13b). This framework prevents extensive mixing of hydrothermal fluid with ambient seawater, and allows pyrrhotite, zinc sulfide, isocubanite, and galena to precipitate interstitially to anhydrite and stevensite. Zinc sulfide nucleates on, and partly replaces, pre-existing pyrrhotite. Isocubanite replaces and is largely co-depositional with zinc sulfide, as seen by its arborescent and plumose intergrowths with zinc sulfide and its presence as extremely fine-grained inclusions in that mineral. With decreasing temperature, chalcopyrite unmixes from isocubanite to form lensoid lamellae. Galena is consanguineous with zinc sulfide and isocubanite/chalcopyrite, and locally replaces both pyrrhotite and zinc sulfide.

As high-temperature venting continues, calcite precipitates both interstitially and as a replacement phase (Fig. 13). With time, walls become thick and voids and fractures are sealed, preventing the inward incursion of seawater. As mixing across chimney walls is inhibited, vent fluids become hotter, and sulfides continue to precipitate internally and to replace non-sulfides in external zones. In old chimneys, the central orifice eventually becomes clogged by precipitation of high-temperature sulfides, resulting in a spire. Fractures which develop in a chimney result in the lateral escape of vent fluid. The buoyant fluid rises and, as it escapes, bathes the chimney surface immediately above the fracture, causing the precipitation of anhydrite and stevensite as an incipient eave (Fig. 13c,d). With conductive cooling and decreasing temperature, amorphous silica coats all primary phases and replaces some minerals in the outer portions of the chimney or spire. The precipitation of minerals such as barite and amorphous silica, and to some degree calcite, which are largely insoluble in cold seawater, results in the growth of extremely large and complex structures (*e.g.*, Fig. 3a,b). Dense clusters of tube worms likely play a role in mineral precipitation and chimney growth by insulating vent fluid from cold, ambient seawater, and by promoting the deposition of higher temperature sulfides and calcite. In some samples, worm tubes are completely encased and replaced by minerals.

The formation of large mounds cannot result solely from high-temperature venting. Converse *et al.* (1984) and McConachy (1988) have estimated that most particulate material in a black-smoker plume is dispersed widely and does not contribute to the formation of the mound. On the other hand, chimney talus and reworked sulfide sediment do play a minor but important role in mound construction. Guaymas mounds are thought to form in a manner analogous to chimneys. Hydrothermal fluid emanating from the basin floor through fissures may precipitate an anhydrite + stevensite cap (Fig. 13), not unlike that envisaged by Campbell *et al.* (1984). As hydrothermal fluids continue to flow through the system, the sediments adjacent to the fissure heat up, and calcite and barite are precipitated as veinlets and in the cap. Once formed, this cap serves as a physical and thermal barrier to mixing of hydrothermal fluid and seawater. Cooling within the incipient mounds is largely by conduction, leading to the precipitation of amorphous silica. Metal-rich fluids penetrating the mounds from below cannot rapidly mix with seawater; sulfides are precipitated interstitially and replace non-sulfide phases. The mound grows by the upward migration of the amorphous silica (+ barite), resulting in the dissolution of the lower part of the siliceous crust and reprecipitation on top. Spires so weakened collapse, and the sediment contributes to the growth of the mound. Figure 13d depicts a mature, fully-developed mound with many of the features observed from ALVIN.

Acknowledgements

Samples used in this study were obtained during the *Pluto 6* cruise to Guaymas Basin (P.F. Lonsdale, chief scientist) with the submersible ALVIN and support vessel *R/V Lulu*. We thank shipboard scientists, the ALVIN group, and crew members for technical support at sea. E.T.C. Spooner and T.J. Barrett provided valuable advice and critically reviewed the first author's M.Sc. thesis, on which this paper is based. This work has benefitted greatly from discussions with W.C. Shanks, B.R.T. Simoneit, M.P. Gorton, T.F. McConachy, M.D. Hannington, D.R. Burrows and L.T. Bryndzia. Expert photography and drafting were provided by B. O'Donovan and S. Shanbag, respectively. This study was funded by the Natural Sciences and Engineering Research Council of Canada through grants to S.D. Scott. Financial support to Peter was also provided by a University of Toronto Open Fellowship and an H.V. Ellsworth Graduate Scholarship in mineralogy.

References

Barton, P.B., Jr. (1978): Some ore textures involving sphalerite from the Furutobe mine, Akita Prefecture, Japan. *Mining Geol.* **28**, 293-300.

_____ & Bethke, P. (1987): Chalcopyrite disease in sphalerite: Pathology and epidemiology. *Amer. Mineral.* **72**, 451-467.

Blount, C.N. & Dickson, F.W. (1969): The solubility of anhydrite ($CaSO_4$) in $NaCl$-H_2O from 100 to 450°C and 1 to 100 bars. *Geochim. Cosmochim. Acta* **33**, 227-245.

Bodnar, R.J. & Bethke, P.M. (1984): Systematics of stretching of fluid inclusions I: Fluorite and sphalerite at 1 atmosphere confining pressure. *Econ. Geol.* **79**, 141-161.

Bowers, T.S., Campbell, A.C., Measures, C.I., Spivack, A.J., Khadem, M. & Edmond, J.M. (1988): Chemical controls on the composition of vent

fluids at 13°N–11°N and 21°N, East Pacific Rise. *J. Geophys. Res.* **93**, 4522-4536.

_____, VON DAMM, K.L. & EDMOND, J.M. (1985): Chemical evolution of mid-ocean ridge hot springs. *Geochim. Cosmochim. Acta* **49**, 2239-2252.

BRETT, R., HEDENQUIST, J.W. & EVANS, H.T., JR. (1985): Sulfide chimneys from S. Juan de Fuca Ridge: Mineralogy and fluid inclusions. *EOS, Trans. Amer. Geophys. Union* **66**, 927.

BRINDLEY, G.W. (1980): Order–disorder in clay mineral structures. *In* Crystal Structures of Clay Minerals and their X-ray Identification (G.W. Brindley & G. Brown, eds.). Mineralogical Society, London, 125-195.

_____, BISH, D.L. & WAN, H-M. (1977): The nature of kerolite, its relation to talc and stevensite. *Mineral. Mag.* **41**, 443-452.

BRYNDZIA, L.T., SCOTT, S.D. & FARR, J.E. (1983): Mineralogy, geochemistry, and mineral chemistry of siliceous ore and altered footwall rocks in the Uwamuki 2 and 4 deposits. *Econ. Geol. Monogr.* **5**, 507-522.

CABRI, L.J. (1973): New data on phase relations in the Cu–Fe–S system. *Econ. Geol.* **68**, 443-454.

_____, HALL, S.R., SZYMAŃSKI, J.T. & STEWART, J.M. (1973): On the transformation of cubanite. *Can. Mineral.* **12**, 33-38.

CALVERT, S.E. (1966): Accumulation of diatomaceous silica in the sediments of the Gulf of California. *Geol. Soc. Amer. Bull.* **77**, 569-596.

CAMPBELL, I.H., MCDOUGALL, T.J. & TURNER, J.S. (1984): A note on fluid dynamic processes which can influence the deposition of massive sulfides. *Econ. Geol.* **79**, 1905-1913.

CHEN, C-T.A. & MARSHALL, W.L. (1982): Amorphous silica solubilities IV. Behavior in pure water and aqueous sodium chloride, sodium sulfate, magnesium chloride, and magnesium sulfate solutions up to 350°C. *Geochim. Cosmochim. Acta* **46**, 279-287.

CONVERSE, D.R., HOLLAND, H.D. & EDMOND, J.M. (1984): Flow rates in the axial hot springs of the East Pacific Rise (21°N): Implications for the heat budget and the formation of massive sulphide deposits. *Earth Planet. Sci. Lett.* **69**, 159-175.

COOKE, R.C. & KEPKAY, P.E. (1980a): The solubility of aragonite in seawater – I. Effect of pH and water chemistry at one atmosphere. *Geochim. Cosmochim. Acta* **44**, 1071-1075.

_____ & _____ (1980b): Solubility of aragonite in seawater – II. Effect of pressure on the onset and maintenance of dissolution. *Geochim. Cosmochim. Acta* **44**, 1077-1080.

CRAIG, J.R. & SCOTT, S.D. (1974): Sulfide phase equilibria. *In* Sulfide Mineralogy: Reviews in Mineralogy **1** (P.H. Ribbe, ed.), 33-38.

CRAWFORD, M.L., KRAUS, D.W. & HOLLISTER, L.S. (1979): Petrologic and fluid inclusion study of calc-silicate rocks, Prince Rupert, British Columbia. *Amer. J. Sci.* **279**, 1135-1159.

EINSELE, G. (1982): Mechanism of sill intrusion into soft sediments and expulsion of pore water. *Initial Reports of the Deep Sea Drilling Project* (J.R. Curray *et al.*, eds.) **64**, 2, 1169-1176. U.S. Gov. Printing Office, Washington, D.C.

_____ (1985): Basaltic sill–sediment complexes in young spreading centers: genesis and significance. *Geology* **13**, 249-252.

_____ (1986): Interaction between sediments and basalt injections in young Gulf of California-type spreading centers. *Geol. Rundschau* **75**, 197-208.

_____, GIESKES, J.M., CURRAY, J., MOORE, D.G., AGUAYO, E., AUBRY, M.P., FORNARI, D., GUERRERO, J., KASTNER, M., KELTS, K., LYLE, M., MATOBA, Y., MOLINA-CRUZ, A., NIEMITZ, J., RUEDA, J., SAUNDERS, A., SCHRADER, H., SIMONEIT, B. & VACQUIER, V. (1980): Intrusion of basaltic sills into highly porous sediments, and resulting hydrothermal activity. *Nature* **283**, 441-445.

ELLIS, A.J. (1963): The solubility of calcite in sodium chloride solutions at high temperatures. *Amer. J. Sci.* **261**, 259-267.

FOLEY, N.K. (1986): Fluid inclusion study of ores from the Fukazawa Mine, Hokuroku District, Akita Prefecture, Japan. *Mining Geol.* **36**, 11-20.

GERRARD, R. (1966): Salinity in the ocean. *In* The Encyclopedia of Oceanography (R.W. Fairbridge, ed.). Van Nostrod Reinhold Company, Toronto.

GOLDHABER, M.B. (1974): *Equilibrium and Dynamic Aspects of the Marine Geochemistry of Sulfur.* Ph.D. thesis, Univ. California, Los Angeles, California.

HATHAWAY, J.C. (1979): Clay Minerals. *In* Marine Minerals. Mineral. Soc. Amer. Short Course Notes **6** (P.H. Ribbe ed.).

HAYMON, R.M. (1983): Growth history of hydrothermal black smoker chimneys. *Nature* **301**, 695-698.

HOLLAND, R.A.G., BRAY, C.J. & SPOONER, E.T.C. (1978): A method for preparing doubly polished thin sections suitable for microthermometric examination of fluid inclusions. *Mineral. Mag.* **42**, 407-408.

HUTCHISON, M.N. & SCOTT, S.D. (1983): Experimental calibration of the sphalerite cosmobarometer. *Geochim. Cosmochim. Acta* **47**, 101-108.

JANECKY, D.R. & SEYFRIED, W.E., JR. (1984): Formation of massive sulfide deposits on oceanic ridge crests: Incremental reaction models for mixing between hydrothermal solutions and seawater. *Geochim. Cosmochim. Acta* **48**, 2723-2738.

JONES, J.B. & SEGNIT, E.R. (1971): The nature of opal. I. Nomenclature and constituent phases. *J. Geol. Soc. Australia* **18**, 56-68.

_____ & _____ (1975): Nomenclature and the structure of natural disordered (opaline) silica. *Contr. Mineral. Petrology* **51**, 231-234.

JUNIPER, S.K. & FOUQUET, Y. (1988): Filamentous iron-silica deposits from modern and ancient hydrothermal sites. *Can. Mineral.* **26**, 859-869.

KIM, K.-R., WELHAN, J.A. & CRAIG, H. (1984): The hydrothermal vent fields at 13°N and 11°N on the East Pacific Rise: ALVIN 1984 results. *EOS, Trans. Amer. Geophys. Union* **65**, 973.

KISSIN, S.A. & SCOTT, S.D. (1982): Phase relations involving pyrrhotite below 350°C. *Econ. Geol.* **77**, 1739-1754.

KOSKI, R.A., LONSDALE, P.F., SHANKS, W.C., BERNDT, M.E. & HOWE, S.S. (1985): Mineralogy and geochemistry of a sediment-hosted hydrothermal sulfide deposit from the Southern Trough of Guaymas

Basin, Gulf of California. *J. Geophys. Res.* **90**, 6695-6707.

LAWVER, L.A. & WILLIAMS, D.L. (1979): Heat flow in the central Gulf of California. *J. Geophys. Res.* **84**, 3465-3478.

_____, _____ & VON HERZEN, R.P. (1975): A major geothermal anomaly in the Gulf of California. *Nature* **257**, 23-28.

LE BEL, L. & OUDIN, E. (1982): Fluid inclusion studies of deep-sea hydrothermal sulphide deposits on the East Pacific Rise near 21°N. *Chem. Geol.* **37**, 129-136.

LONSDALE, P. (1978): Submersible exploration of Guaymas Basin: A preliminary report of the Gulf of California 1977 operations of DSV-4 "Seacliff". *SIO Ref.* **78-1** (Reports, Scripps Inst. Oceanography), La Jolla, Calif.

_____ (1980): Hydrothermal plumes and baritic sulfide mounds at a Gulf of California spreading center. *EOS, Trans. Amer. Geophys. Union* **61**, 995.

_____ (1985): A transform continental margin rich in hydrocarbons, Gulf of California. *Bull. Amer. Assoc. Petrol. Geol.* **69**, 1160-1180.

_____ & BECKER, K. (1985): Hydrothermal plumes, hot springs, and conductive heat flow in the Southern Trough of Guaymas Basin. *Earth Planet. Sci. Lett.* **73**, 211-225.

_____ & LAWVER, L.A. (1980): Immature plate boundary zones studied with a submersible in the Gulf of California. *Geol. Soc. Amer. Bull.* **91**, 555-569.

_____, BISCHOFF, J.L., BURNS, V.M., KASTNER, M. & SWEENEY, R.E. (1980): A high-temperature hydrothermal deposit on the seabed at a Gulf of California spreading center. *Earth Planet. Sci. Lett.* **49**, 8-20.

LUPTON, J.E. (1979): Helium-3 in the Guaymas Basin: Evidence for injection of mantle volatiles in the Gulf of California. *J. Geophys. Res.* **84**, 7446-7452.

MANN, H.B. & WHITNEY, D.R. (1947): On a test of whether one of two variables is stochastically larger than the other. *Ann. Math. Statist.* **18**, 52-54.

MCCONACHY, T.F. (1988): *Hydrothermal Plumes Over Spreading Ridges and Related Deposits in the Northeast Pacific Ocean: The East Pacific Rise Near 11°N and 21°N, Explorer Ridge and J. Tuzo Wilson Seamounts.* Ph.D. thesis, Univ. Toronto, Toronto, Ontario.

MCDONALD, A.J. & SPOONER, E.T.C. (1981): Calibration of a Linkam TH600 programmable heating-cooling stage for microthermometric examination of fluid inclusions. *Econ. Geol.* **76**, 1248-1258.

MICHARD, G., ALBAREDE, F., MICHARD, A., MINISTER, J.-F., CHARLOU, J.-L. & TAN, N. (1984): Chemistry of solutions from the 13°N East Pacific Rise hydrothermal site. *Earth Planet. Sci. Lett.* **67**, 297-307.

MIKAIYAMA, H. & ISAWA, E. (1970): Phase relations in the Cu–Fe–S system. The copper deficient part. *In* Volcanism and Ore Genesis (T. Tatsumi, ed.). Tokyo University Press, 339-355.

MUROWCHICK, J.B. & BARNES, H.L. (1986): Marcasite precipitation from hydrothermal solutions. *Geochim. Cosmochim. Acta* **50**, 2615-2629.

NICKEL, E. (1978): The present status of cathode luminescence as a tool in sedimentology. *Minerals Sci. Eng.* **10**, 73-100.

OUDIN, E. (1983): Hydrothermal sulfide deposits of the East Pacific Rise (21°N) Part 1: descriptive mineralogy. *Mar. Mining* **4**, 39-72.

PETER, J.M. (1986): *Genesis of Hydrothermal Vent Deposits in the Southern Trough of Guaymas Basin, Gulf of California: a Mineralogical and Geochemical Study.* M.Sc. thesis, Univ. Toronto, Toronto, Ontario.

_____ & SCOTT, S.D. (1987): Aqueous and hydrocarbon inclusions in hydrothermal vent deposits of the Guaymas Basin, Gulf of California. *Programs and Abstracts, American Current Research on Fluid Inclusions,* January 1987, Socorro, New Mexico, unpaginated abstr.

_____, _____, SHANKS, W.C., III & WOODRUFF, L.G. (1986): Geochemical, mineralogical, fluid inclusion, and stable isotope studies of hydrothermal vent precipitates, Guaymas Basin, Gulf of California. *In* The Genesis of Stratiform Sediment-hosted Lead and Zinc Deposits: Conference Proceedings (R.J.W. Turner & M.T. Einaudi, eds.). Stanford University Publications, Geol. Sci. **20**, 151-155.

_____, KAWKA, O.E., SCOTT, S.D. & SIMONEIT, B.R.T. (1988): Liquid hydrocarbon-bearing inclusions in modern hydrothermal chimneys and mounds from the Southern Trough of Guaymas Basin, Gulf of California. *In* Third Chemical Congress of North America Symposium: Organic Matter in Hydrothermal Systems – Maturation, Migration and Biogeochemistry. June 1988, Toronto, Canada, Program and Abstracts (abstr.).

PISUTHA-ARNOND, V. & OHMOTO, H. (1983): Thermal history, and chemical and isotopic compositions of the ore-forming fluids responsible for the Kuroko massive sulfide deposits in the Hokuroku District of Japan. *Econ. Geol. Monogr.* **5**, 523-558.

POTTER, R.W. (1977): Pressure corrections for fluid-inclusion homogenization temperatures based on the volumetric properties of the system NaCl-H_2O. *J. Res. U.S. Geol. Surv.* **5**, 603-607.

_____, CLYNNE, M.A. & BROWN, D.L. (1978): Freezing point depression of aqueous sodium chloride solutions. *Econ. Geol.* **73**, 284-285.

ROEDDER, E. (1984): *Fluid Inclusions. Reviews in Mineralogy* **12** (P.H. Ribbe, ed.), Mineral. Soc. Amer., 646p.

SCOTT, S.D. (1985): Seafloor polymetallic sulfide deposits: ancient and modern. *Mar. Mining* **5**, 191-212.

_____ & BARNES, H.L. (1971): Sphalerite geothermometry and geobarometry. *Econ. Geol.* **66**, 653-669.

_____ & _____ (1972): Sphalerite–wurtzite equilibria and stoichiometry. *Geochim. Cosmochim. Acta* **36**, 1275-1295.

SHEPHERD, T.J. (1981): Temperature-programmable, heating-freezing stage for microthermometric analysis of fluid inclusions. *Econ. Geol.* **76**, 1244-1247.

SIEGEL, S. (1956): *Nonparametric Statistics for the Behavioral Sciences.* McGraw-Hill Inc., New York.

SIMONEIT, B.R.T. & LONSDALE, P. (1982): Hydrothermal petroleum in mineralized mounds at the seabed of Guaymas Basin. *Nature* **295**, 198-202.

STYRT, M.M., BRACKMANN, A.J., HOLLAND, H.D. & CLARK, B.C. (1981): The mineralogy and isotopic composition of sulphur in hydrothermal sulphide/sulphate deposits of the East Pacific Rise, 21°N latitude. *Earth Planet. Sci. Lett.* **53**, 382-390.

SUGAKI, A., SHIMA, H., KITAKAZE, A. & HARADA, H. (1975): Isothermal phase relations in the system Cu–Fe–S under hydrothermal conditions at 350°C and 300°C. *Econ. Geol.* **75**, 742-751.

THORNTON, E.C. & SEYFRIED, W.E., JR. (1987): Reactivity of organic-rich sediment in seawater at 350°C, 500 bars: Experimental and theoretical constraints and implications for the Guaymas Basin hydrothermal system. *Geochim. Cosmochim. Acta* **51**, 1997-2010.

TIVEY, M.K. & DELANEY, J.R. (1986): Growth of large sulphide structures on the Endeavor Segment of the Juan de Fuca Ridge. *Earth Planet. Sci. Lett.* **77**, 303-317.

VON DAMM, K.L. & BISCHOFF, J.L. (1987): Chemistry of hydrothermal solutions from the southern Juan de Fuca Ridge. *J. Geophys. Res.* **92**, 11334-11346.

———, EDMOND, J.M., MEASURES, C.I. & GRANT, B. (1985): Chemistry of submarine hydrothermal solutions at Guaymas Basin, Gulf of California. *Geochim. Cosmochim. Acta* **49**, 2221-2237.

WELHAN, J.A. & CRAIG, H. (1982): Abiogenic methane in mid-ocean ridge hydrothermal fluids. *In* Deep Source Gas Workshop Technical Proceedings (W.J. Givilliam, ed.). Morgantown, West Virginia, 122-129.

WIGGINS, L.B. & CRAIG, J.R. (1980): Reconnaissance of the Cu–Fe–Zn–S system sphalerite relationship. *Econ. Geol.* **75**, 742-751.

WILLIAMS, D.L., BECKER, K., LAWVER, L.A. & VON HERZEN, R.P. (1979): Heat flow at the spreading centers of the Guaymas Basin, Gulf of California. *J. Geophys. Res.* **84**, 6757-6769.

ZIERENBERG, R.A., SHANKS, W.C., III & BISCHOFF, J.L. (1984): Massive sulfide deposits at 21°N, East Pacific Rise: Chemical composition, stable isotopes, and phase equilibria. *Geol. Soc. Amer. Bull.* **95**, 922-929.

Received October 6, 1987; revised manuscript accepted June 9, 1988.